Landslide Hazard Map of Kirkland, WA

Kathryn Teague

A report prepared in partial fulfillment of
the requirements for the degree of

Master of Science
Earth and Space Sciences: Applied Geosciences

University of Washington

December, 2016

Internship coordinator:
Kathy Troost

Reading committee:
Steven Walters
Juliet Crider

MESSAGe Technical Report Number: 042

Executive Summary

Landslides are one of the most significant geohazards in the Puget Sound region and have a history of causing extensive damage to development (Baum, Harp, and Highland, 2007). Mapping landslide hazard areas is imperative in reducing the risk landslides pose to people and property. Given the general importance of landslide mapping, the City of Kirkland, WA is interested in such an assessment with respect to their annexation of 7.5 square miles in the northern portion of the City. In particular, landslide mapping is necessary to update the City's Growth Management Act products for the annexed lands.

The Puget Sound region has been repeatedly glaciated over the last 2.4 million years, resulting in a series of glacial deposits of clay, sand, and till. The Vashon stade of the Fraser glaciation reached the Puget Lowland 17,400 calendar years before present and retreated 16,400 calendar years before present (Troost and Booth, 2008). Fraser-age deposits of glacial outwash sand overlying relatively impermeable glacial silt and clay deposits are particularly prone to failure, especially in saturated conditions, because the clay layers can create perched aquifers (Baum et al., 2007). Landslides tend to be associated with the rainy season in the Puget Lowland (October – May) when groundwater accumulates, adding weight to slopes and causing elevated pore pressures (Shannon and Wilson, Inc., 2007). Coastal landsliding is also common in the area, as wave action erodes and destabilizes the base of slopes (Shipman, 2001).

Protocols developed by Oregon Department of Geology and Mineral Industries (DOGAMI) (2009, 2012) provide an effective model for addressing hazards and risks of landslides in Kirkland, WA. These protocols are used to produce a digital inventory of landslide deposits and to identify areas susceptible to shallow landslides. Using geographical information systems (GIS) in conjunction with aerial imagery, high resolution lidar, and field reconnaissance to identify landslides, landslide flanks and deposits are digitized as polygons, while scarps are digitized as lines. Data for each landslide, including type of movement, geology, and slide depth, is included in the attribute table. Geology, slope, and data from the landslide inventory are inputs to the DOGAMI shallow landslide susceptibility model. Factor of safety is calculated for each geologic unit, and slopes with critical factor of safety values are highlighted to produce a hazard map. Factors of safety between 1.25 and 1.5 are considered moderately hazardous, and factors of safety less than 1.25 are identified as highly hazardous. The factor of safety map is filtered to eliminate manmade features like ditches, small retaining walls, and short road cuts, and then a buffer is applied to include areas adjacent to high hazards.

The resulting landslide hazard map can be used to inform City of Kirkland citizens and staff about highly hazardous areas. Future City planning may use this map as a reference for public utilities, infrastructure, and land use. This map may also aid in mitigating hazards to reduce future losses, and increasing public awareness of risk.

Table of Contents

List of Figures

List of Tables

Acknowledgements

This project was funded by the University of Washington and the City of Kirkland. 2016 lidar data were provided by the City of Kirkland. The author would like to thank readers Steven Walters and Juliet Crider, internship coordinator Kathy Troost, and Paul Stewart, Jenny Gaus, Jeremy McMahan, and Karl Johanssen from the City of Kirkland.

Introduction

Kirkland, Washington is an expanding City within the Puget Lowland, east of Lake Washington (Figure 1). The landscape of the City is influenced by tectonic activity of the Cascadia subduction zone and by a series of glacial advances, which caused scouring of bedrock and deposition of glacial sediments (Troost and Booth, 2008). Steep slopes, characteristic glacial geology, and old landslides and landslide deposits within the Puget Lowland make this area particularly vulnerable to slope instability (e.g. Waldron et al., 1962; Waldron, 1967; Tubbs, 1974; Youngmann, 1979; Yount et al., 1993; Harp et al., 1996; Gerstel et al., 1997; Baum et al., 1998; Baum et al., 2000; Laprade et al., 2000; Shipman, 2001; Wait, 2001).

Landslides present a high risk in the Puget Lowland due to a high population density. In 2011, Kirkland annexed three new neighborhoods (Finn Hill, North Juanita, and Kingsgate), which cover 7.2 square miles in the northern part of the City and include 30,000 residents. This newly annexed portion of the City has several steep and convergent hillslopes, which pose a risk of landslides and resultant property damage and injury. The map produced in this project identifies critical areas of Kirkland that have moderate and high susceptibility to landslides. Mapping "Critical areas" as defined under Washington State law (chapter 36.70A RCW), including geologic hazards, serves to update the City's Growth Management Act (GMA) products, informs citizens of potential risks, and classifies the potential risks to development.

Scope of Work

In this project, I used high-resolution lidar to map landslide hazard areas within the northern annexation of the City of Kirkland, WA. I adopted protocols published by the Oregon Department of Geology and Mineral Industries (DOGAMI) for creating a landslide inventory and for shallow landslide susceptibility mapping. The airborne lidar data used in this study were collected in early 2016, providing digital elevation data at 3 ft-resolution. Creation of the shallow landslide susceptibility map relies on accurate geologic and slope maps. The best available geologic data for the annexation area at the time of this study are from a 1:100,000 geologic map. More detailed geologic mapping for this area is ongoing, and the shallow landslide susceptibility map may be updated once better data are available. I used a 1:6,000 geologic map for the southern part of the City (Troost and Wisher, 2008). The products of this study are intended to identify areas where landslides are most likely to occur, but are not intended as a definitive prediction.

Need for Landslide Hazard Mapping

Prior landslide hazard maps have been created for the City of Kirkland, but these are out of date and were produced prior to the newest lidar data. This project is based on the most recent and highest resolution lidar elevation data available, and provides a more detailed view of where landslides may occur. The Growth Management Act also requires that the City produce an updated geologic hazard map following its 2011 annexation to map "Critical areas," including "Geologically hazardous areas" defined under Washington Administrative Code 365-190-120 as "areas susceptible to erosion, sliding, earthquake, or

other geological events." Geologically hazardous areas pose a threat to the health and safety of citizens and should be mapped to limit risk. The Earth and Space Science department at the University of Washington has a grant from the City to update the geology and hazard maps.

Geologic Setting

The Puget Lowland has been overridden by glaciers at least seven times in the last 2 million years. Glacial and interglacial deposits sit on top of an irregular bedrock surface, and can be zero to thousands of feet deep. Repeated glacial scouring and erosion from subglacial streams has resulted in north-south drumlins and the troughs of Puget Sound (Troost and Booth, 2008).

Deposits in the Puget Lowland commonly have a characteristic sequence of till over advance outwash over Lawton Clay (Galster and Laprade, 1991; Figure 2). A large proglacial lake formed by the Puget Lobe of the Cordilleran ice sheet dammed drainage into the Strait of Juan de Fuca, causing deposition of glaciolacustrine silt and clay, which formed the Lawton Clay. On top of this layer, the advance of the Puget Lobe deposited a thick unit of proglacial fluvial and lacustrine sand, known as the Esperance Sand. The contact between the low permeability Lawton Clay and relatively high permeability Esperance Sand is used to predict areas of relatively low slope stability, because water perched above the clay often contributes to slope failure in the Esperance Sand. Many areas are capped with Vashon Till. Some local deposits of Vashon recessional outwash are found where meltwater streams from the retreating glacier cut large channels and emptied into lakes (Tubbs and Dunne, 1977).

Glacial geology and coastal erosion in the Puget Lowland tend to define where most landslides will occur. Landslides often coincide with the rainy season (Baum, Godt, and Highland, 2008), which occurs between October and May. The Seattle area receives an average of 38 inches of precipitation annually (Chleborad, 2003), and landslides commonly occur after heavy precipitation events (Baum et al., 2007). As groundwater levels are raised by an increase in rainfall or by anthropogenic factors (i.e., irrigation, leaky pipes, septic systems), elevated pore pressure destabilizes slopes and can lead to catastrophic slope failure, especially where thick sand and gravel units overlay relatively impermeable silt or clay beds (Tubbs, 1975). Laprade and others (2000) describe three additional mechanisms that drive slope failure in the Puget Lowland. These are: increases in water content on a hillslope, which add weight to the slope and magnify the driving forces that contribute to failure; increased seepage forces, resulting from groundwater moving through the slope, which similarly reduce slope stability and soil strength; and coastal erosion and fluvial systems, which contribute to landsliding by removing support at the toe of a hillslope and destabilizing the upper units. Shallow landslides involve the failure of a thin layer of slope material, with a failure plane of 15 ft or less as defined by Burns et al. (2012). Common modes of shallow failure are slumps, translational slides, earth flows, or a complex combination of these (Burns et al., 2012).

Landslides can also be triggered by major earthquakes, as in 1949, 1965, and 2001 (Baum, et al., 2007). The Puget Sound area has three main sources of earthquakes: shallow crustal faults (including the Seattle Fault Zone), subduction zone earthquakes resulting from the subduction of the Juan de Fuca plate beneath the North American plate, and deep Benioff zone earthquakes (USGS, 2002).

Methods and Assumptions

I used high-resolution lidar data to produce a landslide inventory and to run a shallow landslide susceptibility model. I created both the landslide inventory and the shallow landslide susceptibility model following the Oregon DOGAMI methods (Burns and Madin, 2009; Burns, et al., 2012). I also used the best available geologic maps as inputs for this study. For the three annexed neighborhoods, Finn Hill, North Juanita, and Kingsgate, the best available geologic map is at the 1:100,000 scale (Washington Department of Natural Resources, 2016), whereas a more detailed 1:6,000 map (Troost and Wisher, 2008) was available for the southern portion of the City.

Landslide Inventory

Lidar data were collected in early 2016 by the City of Kirkland (Figure 3). The data are at 3 ft resolution in the State Plan coordinate system, Washington State Plane North, FIPS Zone 4601, which is standard for King County GIS data.

To create an inventory, I mapped existing landslide scarps and deposits and assigned categorical attributes to each feature, following the DOGAMI protocol. Topographic contour lines overlaid on a semi-transparent slope map with a light-to-dark gradient corresponding to low to high slope helps enhance morphology and define landslide features. I displayed these two maps over a DEM with a stretched color ramp showing the gradient in elevation. Orthophotos of similar age to the lidar aided in distinguishing manmade features that may be mistaken as evidence of landsliding from natural features. Geomorphic signatures of landslides, such as concave slope depressions, steep or vertical scarps, transverse ridges, and hummocky topography, are used to identify landslides (Turner and Schuster, 1996). All spatial data were mapped at a 1:4,000 scale.

Spatial Data

Each mapped landslide contains up to four elements: a landslide deposit polygon, a landslide head scarp and flanks polygon, a line demarcating the upper most extent of the headscarp, and lines indicating internal scarps. Not all mapped landslides necessarily contain each element of data; some portions of landslides may not be visible, and some types of landslides do not have internal scarps. I identified landslide deposits using geomorphic signatures such as hummocky topography, concave slope depressions, and steep or vertical scarps. I digitized steep, near-vertical slopes as scarps, and hummocky, disturbed sediments below the slope break as deposits. With age, landslide scarps and deposits smooth out and become less visible in lidar (LaHusen et al., 2016), meaning older landslides are more difficult to identify.

TABULAR DATA

Along with each spatial feature in the inventory, I compiled tabular attribute data for each mapped landslide. These data attributes included the following: type of movement; classification of material and movement types; confidence of landslide identification; estimated age or time of landslide activity; known date of movement and landslide name; slope angle, head scarp, and fan depth measurements; classification of deep or shallow failure; horizontal distance between scarps; general movement direction and size; area and volume. Data were not available for all categories for each mapped landslide; I assigned a value of "No data" for those categories in such cases.

Type of movement is classified as either fall, topple, slide (rotational or translational), spread, channelized debris flow, earth flow, or complex according to Figure 4. Classification of material and movement type is described according to Table 1. Landslides with a depth to failure plane of 15 ft or less are classified as shallow in the DOGAMI protocol, and all others are classified as deep. Depth to failure plane can be calculated by:

$$h = x \cos\theta \qquad \text{(Eqn. 1)}$$

where:

$h =$ Depth normal to failure plane
$x =$ Head scarp height
$\theta =$ Slope angle

Landslide identification confidence is calculated by rating confidence in four categories of identification: 1) Head scarp, 2) Flanks, 3) Toe, 4) Internal scarps, sag ponds or closed depressions, compression ridges, etc. Each of these categories is given a confidence value between 1 and 10, with a value of 0 for an unidentifiable feature and a value of 10 for a clearly identifiable feature. These values are added up to create a confidence rating with a maximum of 40. Landslides identified with high confidence have a value greater than 30. Moderate confidence values are between 11 and 29, and low confidence identifications have values less than 10. This information is included in the attribute table of the landslide inventory.

General movement direction of each landslide is recorded as an azimuth in degrees. Azimuth is measured from the center of the uppermost headscarp to the center of the toe.

Area and volume of landslide deposits are estimated using polygon geometry in GIS. Once the area is found, volume is calculated by multiplying area and depth (found using Eqn. 1). For debris-flow fans, the volume is found by multiplying the area by one third of the maximum depth to account for their cone shape.

Shallow Landslide Susceptibility Map

The shallow landslide susceptibility map is a combination of the inventory of mapped shallow landslides, and calculated factors of safety, consistent with the DOGAMI protocol. Filters and buffers are applied to the landslide inventory and the factor of safety map to produce four maps of susceptibility zones. These four maps are:

1. Landslide Inventory Zone Map
2. Factor of Safety Map
3. Head Scarp Buffer Map
4. Factor of Safety Buffer Map

Landslide Inventory Zone Map

The landslide inventory zone map is created from the landslide inventory (Figure 5; Appendix A). All mapped landslide deposit polygons and head scarp polygons are converted from vector data into 3 ft-resolution raster data, to match the lidar resolution. Unique identifiers and attribute data for individual scarps are not transferred into the raster dataset, but are still present in the original vector landslide inventory map. Rasters are used here so each of the maps are in the same format and can be easily combined into the final susceptibility map. The scarp and deposit rasters are then reclassified and given a value of 3 (high susceptibility zone) because landslide scarps and deposits are often remobilized and can remobilize existing deposits.

Factor of Safety Map

Factor of safety (FOS), in its simplest form, is the relationship of resisting forces over driving forces on a hillslope. When the resisting forces exceed the driving forces, the FOS is greater than 1 and the slope is theoretically stable. Slopes with a FOS of 1 are critically stable, and slopes with a FOS less than 1 are theoretically unstable (Lancaster, 2013). In engineering and geotechnical communities, slopes with a FOS less than 1.5 are considered potentially unstable because it is impossible to predict with certainty all geotechnical properties present (Turner and Schuster, 1996; Cornforth, 2005). In the present study, slopes with a FOS between 1.25 and 1.5 are considered moderately unstable, and slopes with a FOS less 1.25 are considered highly unstable, as in Burns et al. (2012). The equation for FOS of a saturated slope with cohesion is given as (Burns et al., 2012; Lancaster, 2013):

$$FOS = \frac{c\prime}{\gamma h sin\theta} + \frac{tan\phi\prime}{tan\theta} - \frac{m\gamma_w tan\phi\prime}{\gamma tan\theta} \qquad \text{(Eqn. 2)}$$

where:

c' = Effective cohesion
ϕ' = Effective angle of internal friction
γ = Soil density (unit weight)
γ_w = Groundwater density (unit weight)
h = Depth to failure surface

$$m = \frac{\text{Depth to groundwater}}{\text{Depth to failure surface}}$$
$$\theta = \text{Slope angle (degrees)}$$

This infinite slope model for factor of safety is valid for shallow landslides, where the horizontal distance to the top of the slope is much greater than the soil depth, and where the slope is wide and lateral friction forces on the sides of the soil section are neglected (Lancaster, 2013). Burns et al. (2012) define shallow landslides as less than or equal to 15 ft deep, making the infinite slope model a reasonable assumption. In the first term of Eqn. 2, effective cohesion of the slope is divided by the product of soil density, depth to failure surface, and sine of the slope angle. The second term divides the tangent of the effective angle of internal friction and the tangent of the slope angle. The last term is the product of the groundwater depth ratio, the groundwater density, and the tangent of the effective angle of internal friction, divided by the soil density and the tangent of the slope angle.

To calculate FOS on a cell-by-cell basis in a raster map, data on geology, depth to failure surface, depth to groundwater, and slope angle are needed.

I clipped the 1:100,000 geologic map to cover only the annexed area of the City, and combined it with a 1:6,000 geologic map (Troost and Wisher, 2008) for the lower portion of the City. The combined geologic map was then converted from vector data into raster data with a 3 ft cell size so raster calculations could be performed with a uniform scale. Each geologic unit is given a "Geologic Code" identical to its raster ID value and can be used for raster calculations and queries. Using data from the attribute table, I created a spreadsheet of the geologic units present in the study area and the geotechnical properties of each unit (Table 2). Common geotechnical properties of geologic materials are found from literature specific to the Puget Lowland (Selby, 1985; Savage, Morrissey, and Baum, 2000; Debray and Savage, 2001; Harp, Michael, and Laprade, 2006), and when ranges of values for cohesion and internal friction were given, I chose values at the low end of the range, which would thereby result in a more conservative factor of safety calculation.

I assumed groundwater to be at the ground surface for a conservative estimate and because groundwater height is highly variable. This assumption is reasonable, considering that failure is most likely to occur during or after a heavy rain when groundwater levels will be high. With this assumption, *m* is equal to 1. If available, more accurate data on groundwater level may be used.

Depth to failure plane is assumed to be 15 ft. Burns, et al. (2012) define shallow landslides as having failure planes less than or equal to 15 ft. A higher depth to failure plane produces a lower factor of safety, so the maximum depth of 15 ft is used for a conservative estimate of slope stability. For each geologic unit, *h* is set equal to 15 ft. Troost and Wisher (2008) describe colluvium as having a thickness of 3-15 ft on the slopes in the City. Likewise, for the region, 3-15 ft is a common thickness for colluvial and mass wastage deposits (Troost, oral communication). Geotechnical properties for colluvium are used for the shallow

landslide susceptibility map, rather than properties of the underlying geology, because the maximum depth of shallow landslides is 15 ft.

I produced a slope map in inclination degrees using the high-resolution DEM data. Slope angle is later queried to select angles corresponding to a factor of safety of 1.5 or 1.25 for each geologic unit.

The factor of safety is calculated using the given assumptions and geotechnical properties of each geologic unit present in the study area. To quickly and efficiently calculate the factor of safety for each geologic unit at all slopes between 1° and 90°, I created an Excel spreadsheet splitting up the factor of safety equation into three portions:

$$\frac{c\prime}{\gamma h sin\theta} \quad \text{(Eqn. 3)}$$

$$\frac{tan\phi\prime}{tan\theta} \quad \text{(Eqn. 4)}$$

$$\frac{m\gamma_w tan\phi\prime}{\gamma tan\theta} \quad \text{(Eqn. 5)}$$

$$FOS = \text{(Eqn. 3)} + \text{(Eqn. 4)} - \text{(Eqn. 5)}.$$

Values for cohesion, angle of internal friction, and density are tabulated from previous literature, and FOS was calculated for each slope angle between 1° and 90° at 0.5° intervals (Appendix B). Slope angles that produce a FOS of 1.25 (i.e., high instability) and 1.5 (i.e., moderate instability) within each mapped unit or deposit are presented in Table 2.

To map moderate and high hazard FOS zones, I set up two queries for each geologic unit and corresponding slope values associated with moderate or high susceptibility of failure. The moderate zone query selects the raster cells with a given geologic unit value, slopes greater than or equal to the FOS=1.5 threshold (16.5° in the example below), and slopes less than or equal to the FOS=1.25 threshold (20° in the example below):

$$(\text{"Geologic Unit"} == 2)\ \&\ (\text{"Slope"} \geq 16.5)\ \&\ (\text{"Slope"} \leq 20)$$

The high hazard zone query selects slopes greater than the FOS 1.25 threshold:

$$(\text{"Geologic Unit"} == 2)\ \&\ (\text{"Slope"} > 20)$$

I repeated these queries for each geologic code and its corresponding slope values throughout the study area. The product is a moderate susceptibility map and a high susceptibility map for each unit. Moderate susceptibility zones are reclassified and given a value of 2, and high susceptibility zones are reclassified and given a value of 3. All the reclassified rasters are then combined into a single raster set with values of 2 and 3

indicating moderate and high susceptibility, respectively, and "NoData" indicating low susceptibility. This is the factor of safety map (Figure 6).

Though high resolution lidar is useful in providing detailed data, it can cause fine-scale features such as ditches, small retaining walls, road cuts, and other steep slopes with low vertical relief to be falsely classified as having moderate or high susceptibility. To reduce the over-prediction of low relief slopes, I smoothed the FOS map using focal relief. Using a focal neighborhood analysis with a moving window of 15 square feet, I identified cells with a focal relief greater than 4 ft, assigning values of 1 where focal relief is greater than 4 ft, and 0 where focal relief is less than or equal to 4 ft. Burns et al. (2012) tested various neighborhood and vertical relief values and found 4 ft of vertical relief over a 15 square foot neighborhood to be the most effective in eliminating over prediction. The relief value of 4 ft corresponds to the typical height of small, landscape-type retaining walls. The focal relief raster is multiplied by the FOS map, which effectively clips all areas of the FOS map that have a vertical relief of 4 ft or less.

Convergent hillslopes increase the potential for slope failure, and are rule-identified landforms (RIL) in Washington State (DNR, 2016). RILs are areas identified by the State that are potentially unstable for forest practices due to one or more factors, including steep and convergent slopes or gorges. Though RILs are generally applied for forest practices in mountainous areas, the concept of highlighting convergent areas may be a useful analysis in this setting. I used an analysis of planform convergence, not included in the DOGAMI protocol, to further highlight areas of particular concern in the FOS map. I created a map of planform curvature from the high resolution DEMs, then smoothed this map using a focal mean analysis with a 15 square foot neighborhood window size. I created a Boolean raster with values of 1 for all slopes with a plan curvature less than 0 (i.e., slopes exhibiting local convergence), and 0 otherwise. I overlaid this raster with the clipped FOS map. The result of this process eliminates areas of low vertical relief and areas of planar or divergent curvature from the FOS map to highlight convergent slopes that may be of particular concern. I compared the final susceptibility map including a curvature analysis to the final map without a curvature analysis to see how curvature changed the estimation of hazard areas.

HEAD SCARP BUFFER MAP

Areas directly upslope of landslide head scarps are predisposed to future failures because scarps tend to continue cutting back into the slope over time (e.g., Baum et al., 2000; LaHusen, 2016; Mirus et al., 2016). The loss of resisting forces directly adjacent to and below the head scarp, as well as the steepness of the scarp, contribute to this retrogressive failure (Burns et al., 2012). Although the FOS identifies head scarps as hazard areas, it does not identify the areas above head scarps, which tend to be relatively flat, but would be dangerous to build on. Applying a buffer to known head scarps identifies areas prone to failure that the FOS map does not detect.

I applied a buffer width of 30 ft, twice the depth of failure, to the head scarp layer. A buffer twice the depth of failure is commonly used in geotechnical engineering because this ratio

is equal to a slope of 26°, and most natural, non-landslide, geologic units have an angle of internal friction of at least 26° (Burns et al., 2012). I then converted the buffer polygons into a raster dataset, which is reclassified and given a value of 3 because these areas can be highly hazardous due to the tendency of scarps to continue cutting back into a hillslope.

FACTOR OF SAFETY BUFFER MAP

Areas immediately adjacent to cells with a FOS less than 1.5 are more likely to fail than areas far away from mapped unstable zones. Head scarps commonly fail through regression into the flat area above the slope and landslides run out onto the flat area at the foot of the slope, so there is need for a buffer around low FOS zones (Chorley, Schumm, and Sugden, 1985). I applied a 30 ft buffer (twice the maximum slide depth) to all areas with a FOS of less than or equal to 1.5, and gave the buffered areas a value of 2, or moderate susceptibility.

Results: Landslide Inventory and Hazard Maps

The landslide inventory map is presented in Appendix A, and tabular data is archived within the digital map product. The Central Houghton Neighborhood in the southern portion of the City has the largest mapped landslide deposit. Gullies in the Finn Hill, North Juanita, and Kingsgate Neighborhoods also have mapped landslide deposits. The cumulative area of inventoried deposits is over 77,000 square feet (Table 3), but the actual area of deposits is likely greater because urbanization and modification of the landscape throughout much of Kirkland has likely obscured evidence of past landslides (Crawford, 2011). Similarly, very old landslides may have been missed in the inventory due to the smoothing out of their distinguishing features with age (Gonzalez-Diez et al., 1999; McKean and Roering, 2004). Due to the relative age of the mapped landslides, and urbanization effects, it is difficult to discern landslide types with much confidence. Even in field investigations, landslide deposits are so heavily vegetated that little information can be gathered. Landslides contained in the inventory commonly occur in mapped Quaternary landslide or mass wastage deposits. Locations of these deposits are shown in Figure 7.

The landslide hazard map, combining landslide inventory and factory of safety, is presented in Figure 8, and Figure 9 shows the calculated hazard also accounting for plan curvature of the slopes. I used the landslide hazard maps both with and without a curvature analysis to calculate the amount of moderate and high hazard areas in each (Table 3 and Table 4). The landslide hazard map without curvature analysis has about 1 million square feet of high hazard area, and 1.9 million square feet of moderate hazard area. With the application of a curvature analysis, these values were reduced to about 900,000 square feet of high hazard area and 1.6 million square feet of moderate hazard area. Curvature clipping did not significantly alter areas of the City designated as hazardous, with the Finn Hill neighborhood having the greatest concentration of high hazard zones in both maps. The application of a curvature analysis to the DOGAMI methodology produces a hazard map that highlights convergent areas, with 14% less area of high hazard, and 16% less area of moderate hazard than the original map.

Curvature filtering removed areas of the FOS map that have planar or divergent slopes, but did not substantially alter the larger pattern of hazard areas. For example, on the west side of the Finn Hill neighborhood, the original hazard map identifies nearly entire gullies as high hazard zones. The curvature-clipped map still identifies the majority of these same areas as high hazard zones, but with lower spatial density (Figure 10). Though adding in a curvature analysis creates a more tailored map of susceptibility, this analysis could lead to an under prediction of hazard zones if failure within convergent slopes is likely to affect adjacent planar or divergent slopes. Zones of high convergence already tend to be withdrawn from current development, so it is unlikely that the curvature-clipped map would have significant implications for development.

The threshold slopes corresponding to moderate and high susceptibility zones vary with geology. Aside from sedimentary rock deposits, glacial till has the highest threshold slopes with a 73.5° slope separating the moderate and high zones (Table 2). Glacial drift, advance outwash, and alluvium have the lowest threshold slope value, since these units have little to no cohesion. Units mapped as glacial drift in the 1:100,000 geologic map were given conservative values relating to the geotechnical properties of till, glaciofluvial sediments, and glaciolacustrine sediments since no better data were available (Hicock and Armstrong, 1985). Threshold slopes for drift, outwash, and alluvium range between 12°-13°. Using general values for geotechnical properties of each unit, glacial till will be most stable at high slopes, and outwash and alluvium will be unstable. Threshold slopes for other geologic units are shown in Table 2.

As landslides tend to occur in areas of previous failure and in geologic units with low cohesion and angles of internal friction, landslide deposits (Qls), mass wasting deposits (Qmw), and advance outwash (Qga) are the most susceptible (Figure 7). Analyzing landslide hazard areas by geology using a table of zonal statistics, I found that Qls deposits have the largest density of high hazard zones, followed by Qga, and Qmw. Advance outwash deposits have the highest total count of both moderate and high hazard zones, totaling an area of more than 260,000 square feet. Landslide deposits have nearly 156,000 square feet of moderate and high hazard zones, and mass wasting deposits have about 129,000 square feet of total hazard zones.

The landslide hazard map of the City of Kirkland shows that large portions of the 2011 annexed area have some amount of hazard (Figure 8). Each of the three annexed neighborhoods have several hazard areas.

Most of the steep, lake-shore areas of the Finn Hill neighborhood that border Lake Washington are identified as moderate or highly hazardous by the susceptibility model (Figure 11). Undeveloped areas near Holmes Point and Denny Park are classified as highly susceptible to shallow landslides. Slopes into the Denny Creek gully vary from 16°-26°, and relief into the creek varies from 100 to 300 ft. Other steep areas on the eastern border of Finn Hill near NE 128th Lane are identified as hazardous and have slopes up to 28°, and 50 ft of relief.

Portions of the North Juanita neighborhood have high and moderate landslide hazards, particularly near Juanita High School and Edith Moulton Park (Figure 11). Land bordering Juanita High School has a stair-stepped elevation profile associated with grading and development of the school, giving it up to 70 ft up relief in the northeastern corner, which the model classifies as hazardous. Undeveloped areas within and surrounding Edith Moulton Park have hillslopes with 50-100 ft of relief.

Kingsgate has patches of hazardous areas in the Juanita Creek gully near I-405, and on the eastern border near 137th Place NE (Figure 11). The Juanita Creek gully has relief up to 90 ft and a slope of 12°. The terrain near 137th Place NE is hummocky and has up to 100 ft of relief in places, and slopes up to 17°. There are steep, convergent slopes east of Muir Elementary School.

With more precise geologic data, areas not currently identified as hazardous may change. For example, several gullies in Finn Hill and a broadly convergent area on the northwest shores of Juanita Bay are not marked as hazardous though their geomorphology suggests otherwise. Currently, these areas are mapped as glacial till; however, if this designation changes with the updated geologic map, these areas may be identified as more hazardous than currently listed. Areas such as these that have steep or convergent topography, but that are not identified by the susceptibility model, highlight the importance of the ongoing geologic mapping effort. When a new geologic map is available, this landslide hazard analysis should be updated to produce the most comprehensive product possible.

As the DOGAMI (SP45) protocol focuses on shallow landslides, a susceptibility analysis of deep-seated failures is omitted from this report. Burns and Mickelson (2016) find that deep landslides are most likely to occur within or adjacent to existing deep landslide deposits. Several of the existing scarps mapped in the landslide inventory are classified as deep-seated based on the height of their head scarps, but more work regarding deep landslides is needed. Some of these deep slides are likely very old based on the smoothness of the topography (Gonzalez-Diez, 1999; McKean and Roering, 2004). A DOGAMI protocol (SP48) for deep landslide susceptibility mapping was published in 2016 (Burns and Mickelson, 2016), prior to the work discussed in this report, and may be used in future work to update the landslide hazard map.

Uses for this Map

Information contained within this landslide hazard map is intended to provide insight for staff and citizens of the City, though the map is not a substitute for geological and geotechnical site investigations. With this map, development in susceptible areas can be avoided or properly engineered, landslide risk to existing development can be mitigated, and the City can develop plans for landslide disasters (Burns and Madin, 2009). Other possible uses for this map include planning relating to public utilities, City infrastructure, land use, and emergency response (Harp, Michael, and Laprade, 2006).

Limitations

The hazard map created in this study is useful at a community or regional scale, but is not an alternative to a site-specific assessment. Even though high-resolution lidar aids in producing more accurate landslide inventories than other methods, such as analysis of aerial photography, it is possible that some landslides will be overlooked or misidentified with this method (Haugerud et al., 2003). Anthropogenic activities alter hillslopes and can remove the geomorphic expression of landslides, or can mimic the characteristics of landslides, such as with cut and fill slopes (Burns and Madin, 2009). Either case impacts the accuracy of the landslide inventory.

Lidar-based elevation data impact the accuracy of this hazard map because there is no ability to distinguish between elevation changes that are due to infrastructure and those that are natural. Misidentification of manmade features as landslide features may cause an overestimate of susceptibility, and though the focal relief method is used to clip some areas of the map where features are misidentified, overestimation is still a possibility where development such as cut and fills and small landscaping retaining walls are misidentified. Similarly, underestimation of susceptibility in areas adjacent to those with low FOS values may be an issue in isolated cases, despite buffers that attempt to correct for this.

The assumed values for depth to groundwater and depth to failure surface used in FOS calculations may not accurately represent local conditions. Depth to groundwater, for example, can vary widely within a small area. I assumed conservative, limiting cases for the values in this study to represent the worst-case scenario, but these values will not necessarily represent all local conditions well, particularly in the dry season.

With more detailed inputs from future data, this landslide hazard map may be improved. The best available geologic data for the annexation area of Kirkland at the time of this study is a 1:100,000 scale map, which is coarser than ideal for this type of work. An ongoing project to create a detailed geologic map of this area will allow this hazard map to be updated in future work. Lidar used in this study was collected in early 2016, but any topographic changes or new landslides that occurred after this date may render portions of this map inaccurate.

Conclusions

Lidar-derived high-resolution elevation data, an infinite slope analysis of stability, and a landslide inventory were used to produce a landslide hazard map for Kirkland, Washington. In the landslide inventory, head scarps and deposits were mapped as polygons, and internal scarps were mapped as lines. Tabular data, including landslide type and classification, confidence of landslide identification, and movement direction, were recorded for all landslides as available (Burns and Madin, 2009). Factor of safety was calculated for each geologic unit using properties of deposits as reported in the literature (Selby, 1982; Savage et al., 2000; Debray and Savage, 2001; Harp et al., 2006;). Slopes corresponding to FOS values less than 1.25 were considered highly hazardous. Slopes with a FOS between 1.25 and 1.5 were considered moderately hazardous, while those with a FOS greater than 1.5 were considered insignificantly or not hazardous. Buffers were

applied to the FOS map and the landslide inventory map to capture the risk in areas adjacent to highly hazardous areas (Burns et al., 2012). Landslide deposits, mass wasting deposits, and advance outwash were the most susceptible geologic units and had the highest counts of moderate and high hazard zones. I found that introducing a curvature analysis to the DOGAMI protocol decreased the counts of both moderate and high hazard zones, but did not have a large impact on the larger pattern of hazards. Most high hazard zones are in undeveloped parks and gullies, and do not pose a large threat to existing infrastructure. The final landslide hazard map may be used to inform the City of Kirkland of areas that are highly hazardous, and to help make planning and mitigation decisions.

References Cited

Baum, R.L., Chleborad, A.F., and Schuster, R.L., 1998, Landslides triggered by the winter 1996–97 storms in the Puget Lowland, Washington: U.S. Geological Survey Open-File Report 98–239, 16 p.

Baum, R.B., Godt, J.W, and Highland, L., 2008, Landslides and engineering geology of the Seattle, Washington, area: Boulder, Colorado, Reviews in engineering geology: Geological Society of America, v. 20, 181 p.

Baum, R.B., Harp, E., and Highland L., 2007, Landslide hazards in the Seattle, Washington area: U.S. Geological Fact Sheet 2007-3005, 4 p.

Baum, R.L., Harp, E.L., and Hultman, W.A., 2000, Map showing recent and historic landslide activity on coastal bluffs of Puget Sound between Shilshole Bay and Everett, Washington: U.S. Geological Survey Miscellaneous Field Studies Map MF–2346, 1 sheet.

Burns, W.J. and Madin, I.P., 2009, Protocol for inventory mapping of landslide deposits from light detection and ranging (lidar) imagery, DOGAMI Special Paper 42, 36 p.

Burns, W.J., and Mickelson, K.A., 2016, Protocol for deep landslide susceptibility mapping: DOGAMI Special Paper 48, 69 p.

Burns, W.J., Madin, I.P., and Mickelson, K.A., 2012, Protocol for shallow-landslide susceptibility mapping, DOGAMI Special Paper 45, 38 p.

Chleborad, A.F., 2003, Preliminary evaluation of a precipitation threshold for anticipating the occurrence of landslides in the Seattle, Washington, area: U.S. Geological Survey Open-File Report 2003-463.

Chorley, R.J, Schumm, S.A., and Sugden, D.E., 1985, Geomorphology: New York, Methuen, p. 273.

Cornforth, D.H., 2005, Landslides in practice: Investigation, analysis, and remedial/preventative options in soils: Hoboken, N. J., John Wiley and Sons, p. 596.

Crawford, M.M., 2011, Inventory Mapping and Characterization of Landslides Using LiDAR: Kenton and Campbell Counties, Kentucky, in Digital Mapping Techniques '11–12—Workshop Proceedings: U.S. Geological Survey Open-File Report 2014-1167.

Debray, S., and Savage, W.Z., 2001, A preliminary finite-element analysis of a shallow landslide in the Alki area of Seattle, Washington: U.S. Geological Survey Open-File Report 01-0357, 6 p.

Esri, 2016, ArcGIS Online Basemap Data: Aerial Imagery and Streets. Accessible at: https://www.arcgis.com/home/item.html?id=3b93337983e9436f8db950e38a8629af and

https://www.arcgis.com/home/item.html?id=10df2279f9684e4a9f6a7f08febac2a9
.

Galster, R.W., and Laprade, W.T., 1991, Geology of Seattle, Washington, United States of America: Bulletin of the Association of Engineering Geologists, v. 28, no. 3, p. 235-302.

Gerstel, W.J., Brunengo, M.J., Lingley, W.S., Jr., Logan, R.L., Shipman, Hugh, and Walsh, T.J., 1997, Puget Sound bluffs: the where, why, and when of landslides following the holiday 1996/97 storms: Washington Geology, v. 25, no. 1, p. 17–31.

Gonzalez-Diez, A., Remondo, J., Diaz de Teran, J., and Cendrero, A., 1999, A methodological approach for the analysis of the temporal occurrence and triggering factors of landslides: Geomorphology, vol. 30(1-2), p. 95–113.

Harp, E.L., Chleborad, A.F., Schuster, R.L., Cannon, S.H., Reid, M.E., and Wilson, R.C., 1996, Landslides and landslide hazards in Washington State due to February 5-9, 1996 storm: U.S. Geological Survey Administrative Report, 29 p.

Harp, E.L., Michael, J.A., and Laprade, W.T., 2006, Shallow-Landslide Hazard Map of Seattle, Washington, U.S. Geological Survey Open-File Report 2006-1139, 23 p.

Haugerud, R.A., Harding, D.J., Johnson, S.Y., Harless, J.L., Weaver, C.S., and Sherrod, B.L., 2003, High-resolution lidar topography of the Puget Lowland, Washington: A bonanza for earth science: GSA Today, v. 6, p. 4-10.

Hicock, S.R., and Armstrong, J.E., 1985, Vashon Drift: Definition of the formation in the Georgia Depression, southwest British Columbia: Canadian Journal of Earth Sciences, v. 22, n. 5, p. 748-757.

Highland, L., compiler, 2004, Landslide types and processes, U.S. Geological Fact Sheet 2004-3072 (ver. 1.1), 4 p.

LaHusen, S.R., Duvall, A.R., Booth, A.M., Montgomery, D.R., 2016, Surface roughness dating of long-runout landslides near Oso, Washington (USA), reveals persistent postglacial hillslope instability: Geology, v. 44(2), p. 111-114.

Lancaster, S.T., 2013, Landslides: force balance and soil water, Course Notes for GEO 322 Surface Processes, College of Earth, Ocean, and Atmospheric Sciences, Oregon State University, 13 p.

Laprade, W.T., Kirkland, T.E., Nashem, W.D., and Robertson, C.A., 2000, Seattle landslide study, Shannon and Wilson, Inc. Internal Report W-7992-01, 164 p.

McKean, J., and Roering, J., 2004, Objective landslide detection and surface morphology mapping using high-resolution airborne laser altimetry: Geomorphology, vol. 57(3-4), p. 331–351.

Mirus, B.B., Smith, J.B., Stark, B., Lewis, Y., Michel, A., and Baum, R.L., 2016, Assessing Landslide Potential on Coastal Bluffs near Mukilteo, Washington—Geologic Site Characterization for Hydrologic Monitoring, U.S. Geological Survey Open-File Report 2016-1082, 34 p.

Savage, W.Z., Morrissey, M.M., and Baum, R.L., 2000, Geotechnical properties for landslide-prone Seattle-area glacial deposits: U.S. Geological Survey Open-File Report 00-228, 6 p.

Selby, M.J., 1982, Hillslope materials and processes: Oxford, Oxford University Press, 264 p.

Shipman, H., 2001, Coastal landsliding on Puget Sound: A review of landslides occurring between 1996 and 1999: Publication #01-06-019, Shorelands and Environmental Assistance Program, Washington Department of Ecology, Olympia, 101 p.

Troost, K.G., and Booth, D.B., 2008, Geology of Seattle and the Seattle area, Washington, *in* Baum, R.L., Godt., J.T., and Highland, L.M., eds., Landslides and Engineering Geology of the Seattle, Washington, Area: Geological Society of America Reviews in Engineering Geology, v. XX, 35 p.

Troost, K.G., and Wisher, A.P., 2008, Geologic Map of Kirkland: Prepared for the City of Kirkland, 1 sheet and 1 table, 1:6,000.

Tubbs, D.W., 1974, Landslides in Seattle: Washington Division of Geology and Earth Resources Information Circular 52, 15 p., 1 plate.

Tubbs, D.W., 1975, Causes, mechanisms, and prediction of landslides in Seattle, Ph.D. Dissertation: University of Washington, 89 p., 1 plate.

Tubbs, D.W., and Dunne, T., 1977, Geologic hazards in Seattle: A field guide for the Geological Society of America Annual Meeting, 23 p.

Turner, A. K., and Schuster, R. L., eds., 1996, Landslides—Investigation and mitigation: Washington, D.C., Transportation Research Board Special Report 247, 673 p.

U.S. Geological Survey, 2002, Cascadia earthquake sources: The Pacific Northwest Urban Corridor Geologic Mapping Project.

Varnes, D.J., 1978, Slope movement types and processes, *in* Schuster, R.L., and Krizek, R.J., eds., Lanslides – Analysis and control: Washington, D.C., Transportation Research Board Special Report 176, p. 11-33.

Wait, T.C., 2001, Characteristics of deep-seated landslides in Seattle, Washington: Golden, Colorado School of Mines, M.S. thesis, 131 p., 3 plates.

Waldron, H.H., 1967, Geologic map of the Duwamish Head quadrangle, King and Kitsap Counties, Washington: U.S. Geological Survey Geologic Quadrangle GQ–706, 1 sheet,

scale 1:24,000.

Waldron, H.H., Leisch, B.A., Mullineaux, D.R., and Crandell, D.R., 1962, Preliminary geologic map of Seattle and vicinity, Washington: U.S. Geological Survey Miscellaneous Geologic Investigations Map I-354, 1 sheet, scale 1:31,680.

Washington State Department of Natural Resources, 2016, Forest practices board manual, S. 16, 93 p.

Youngmann, C. (ed.), 1979, King County: Coastal zone atlas of Washington: Olympia, Washington Department of Ecology, 9 sheets.

Yount, J.C., Minard, J.P., and Dembroff, G.R., 1993, Geologic map of surficial deposits in the Seattle 30' by 60' quadrangle, Washington: U.S. Geological Survey Open-File Report 93–233, 3 sheets.

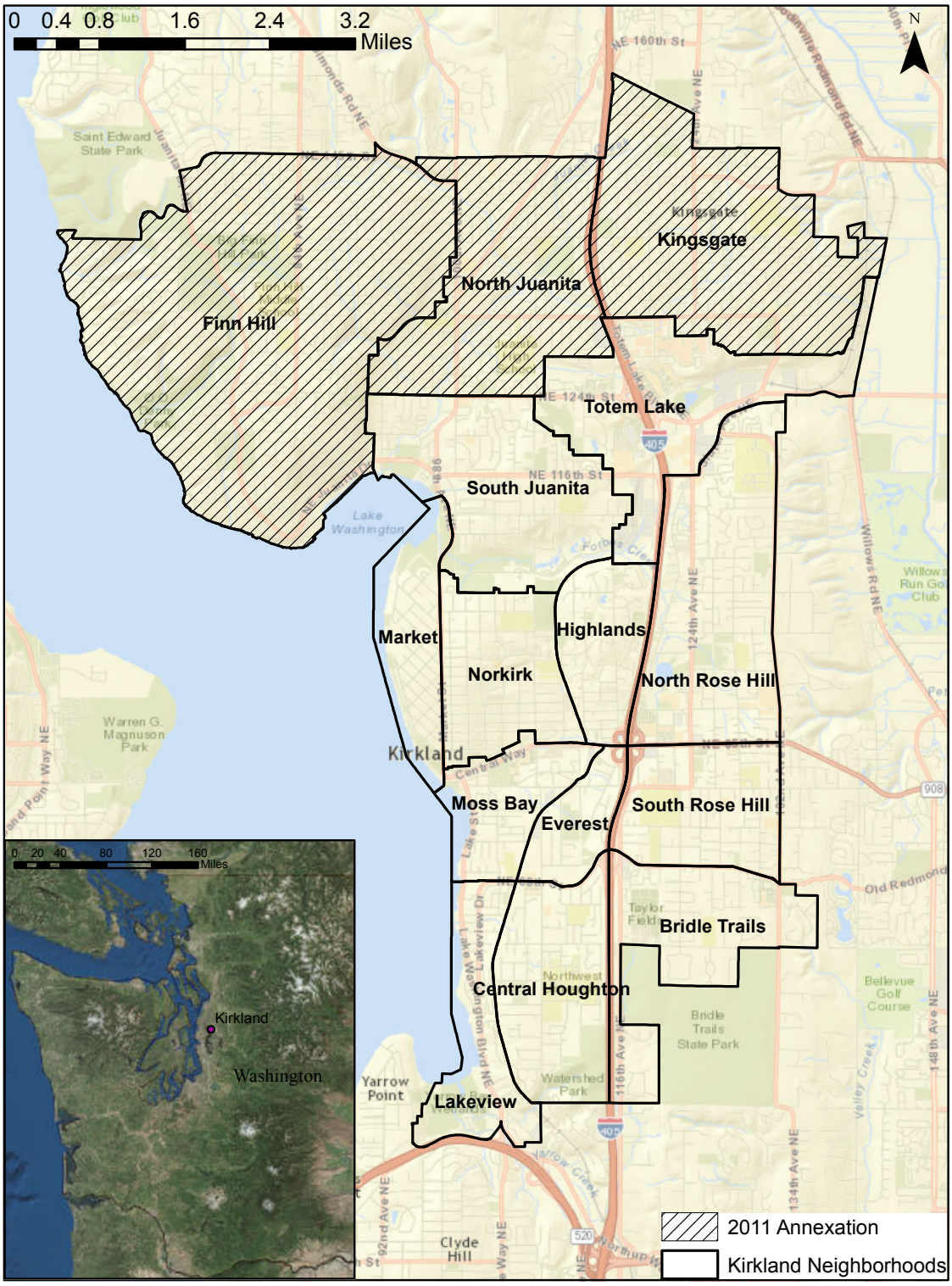

Figure 1. Kirkland neighborhoods and annexed lands, inset of Kirkland in reference to Western Washington State. Basemaps from Esri (2016).

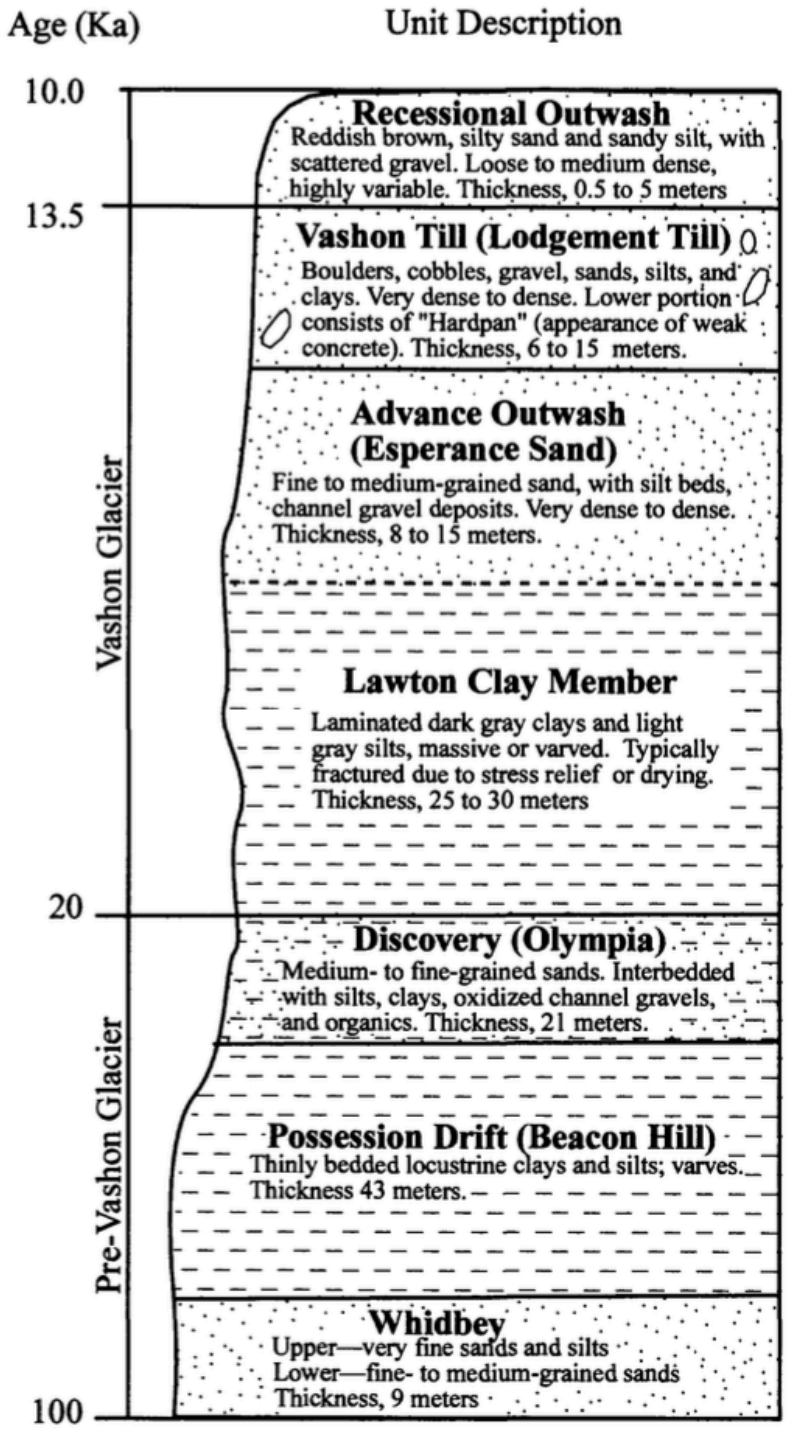

Figure 2. Generalized Seattle-area stratigraphy. Landslides tend to occur at the contact between advance outwash and Lawton Clay (Galster and Laprade, 1991; Savage et al., 2000).

Figure 3. Slope shade of lidar data.

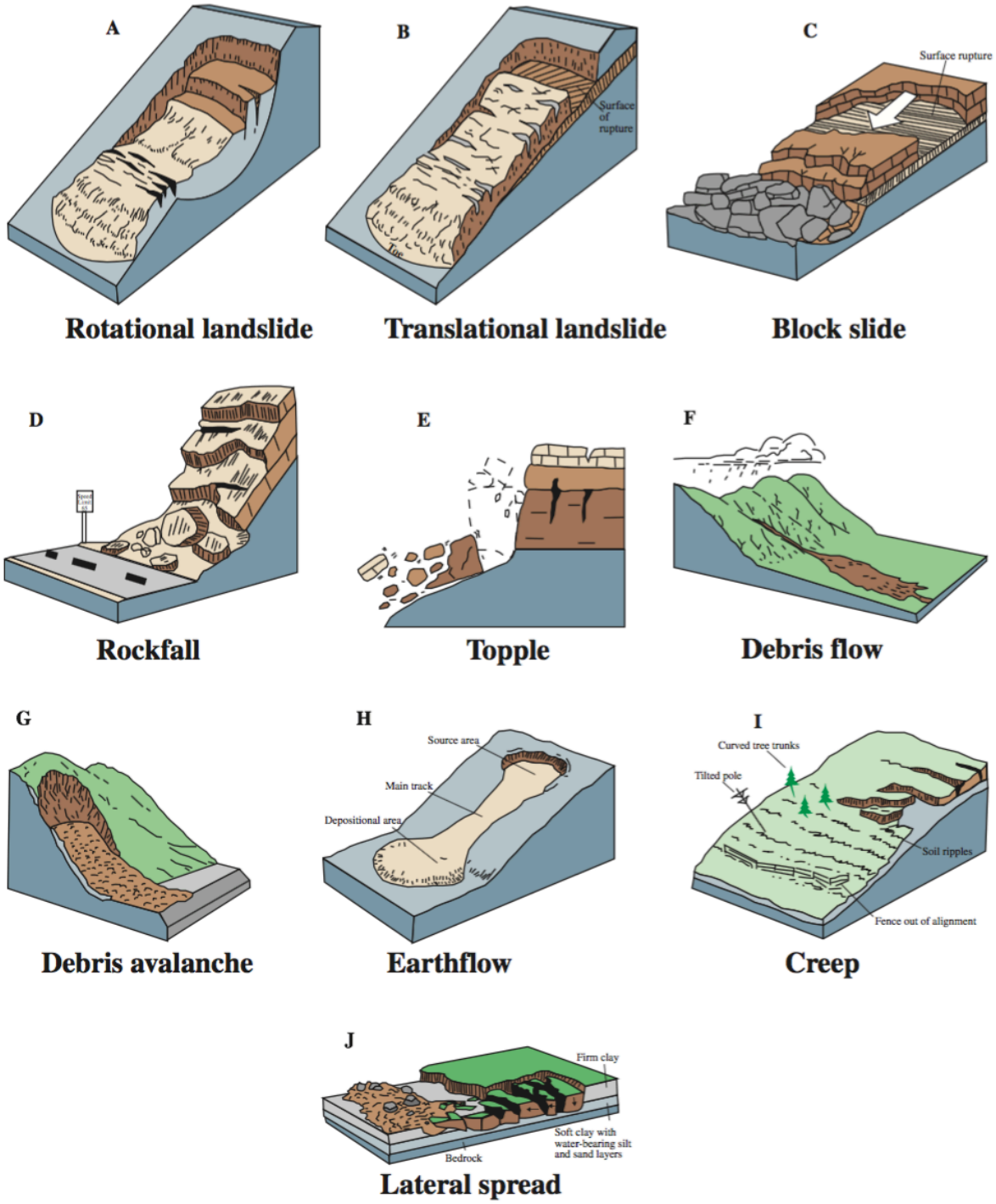

Figure 4. Types of landslides (Highland, 2004).

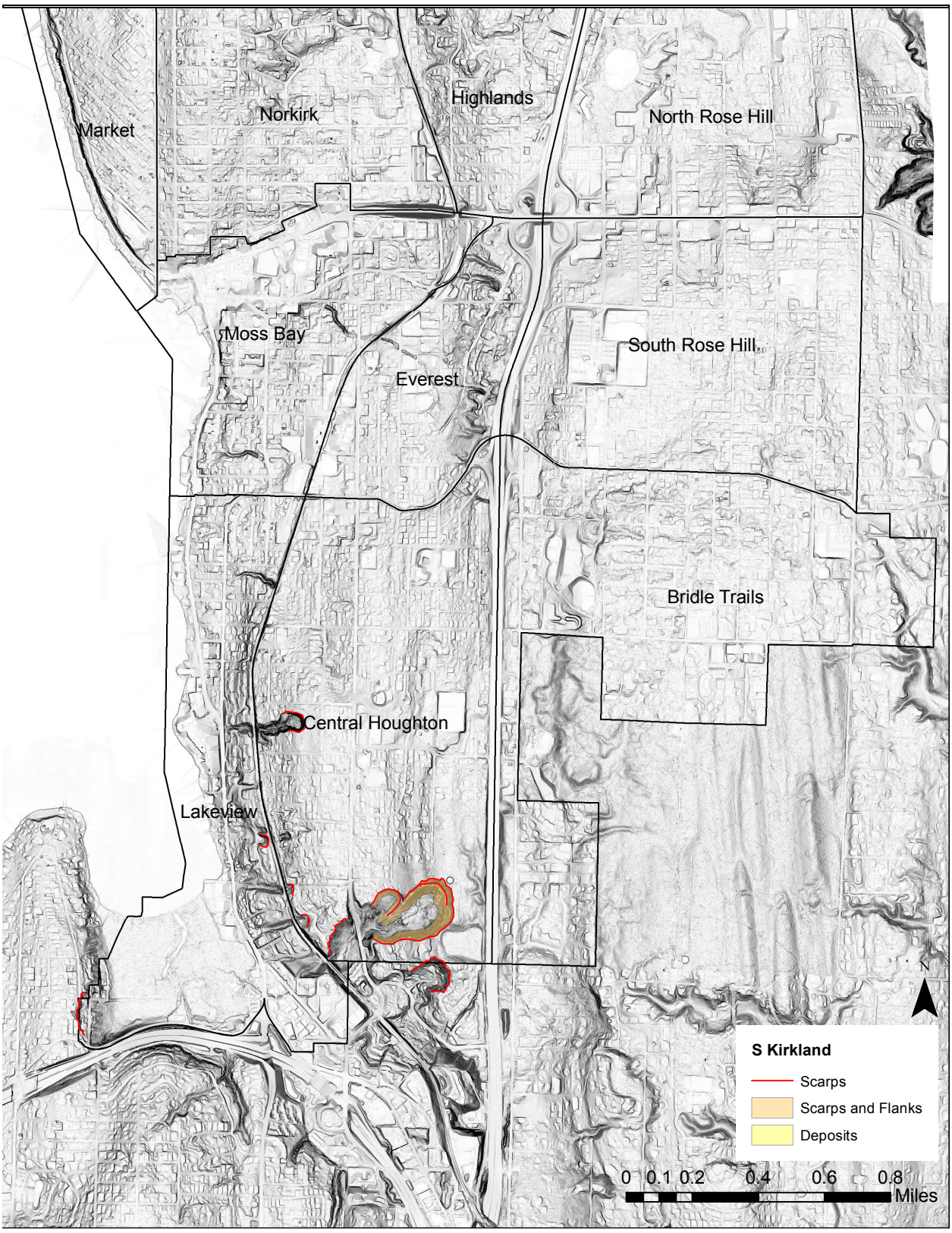

Figure 5. A portion of landslide scarps digitized in the inventory. The entire inventory is shown in Appendix A.

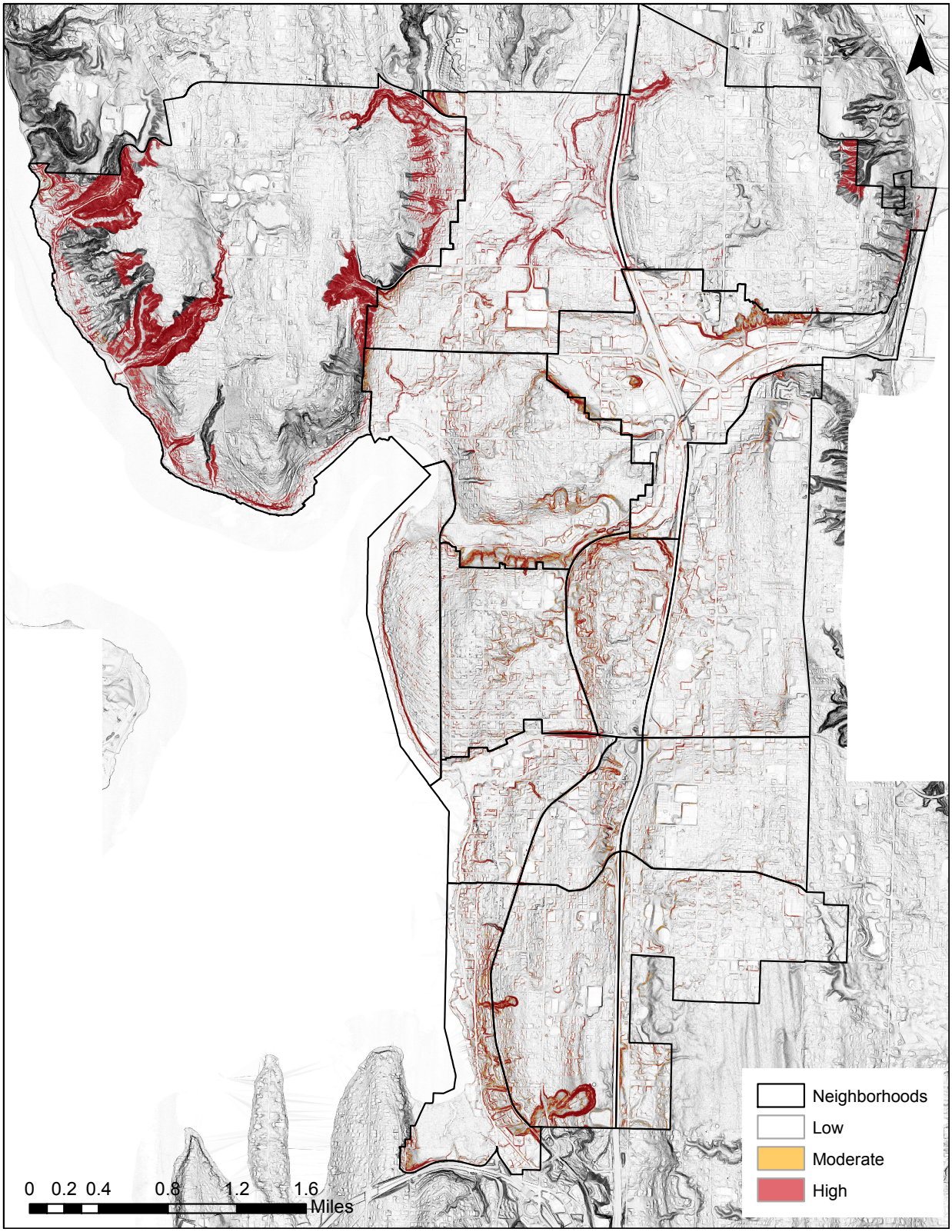

Figure 6. Factor of Safety map.

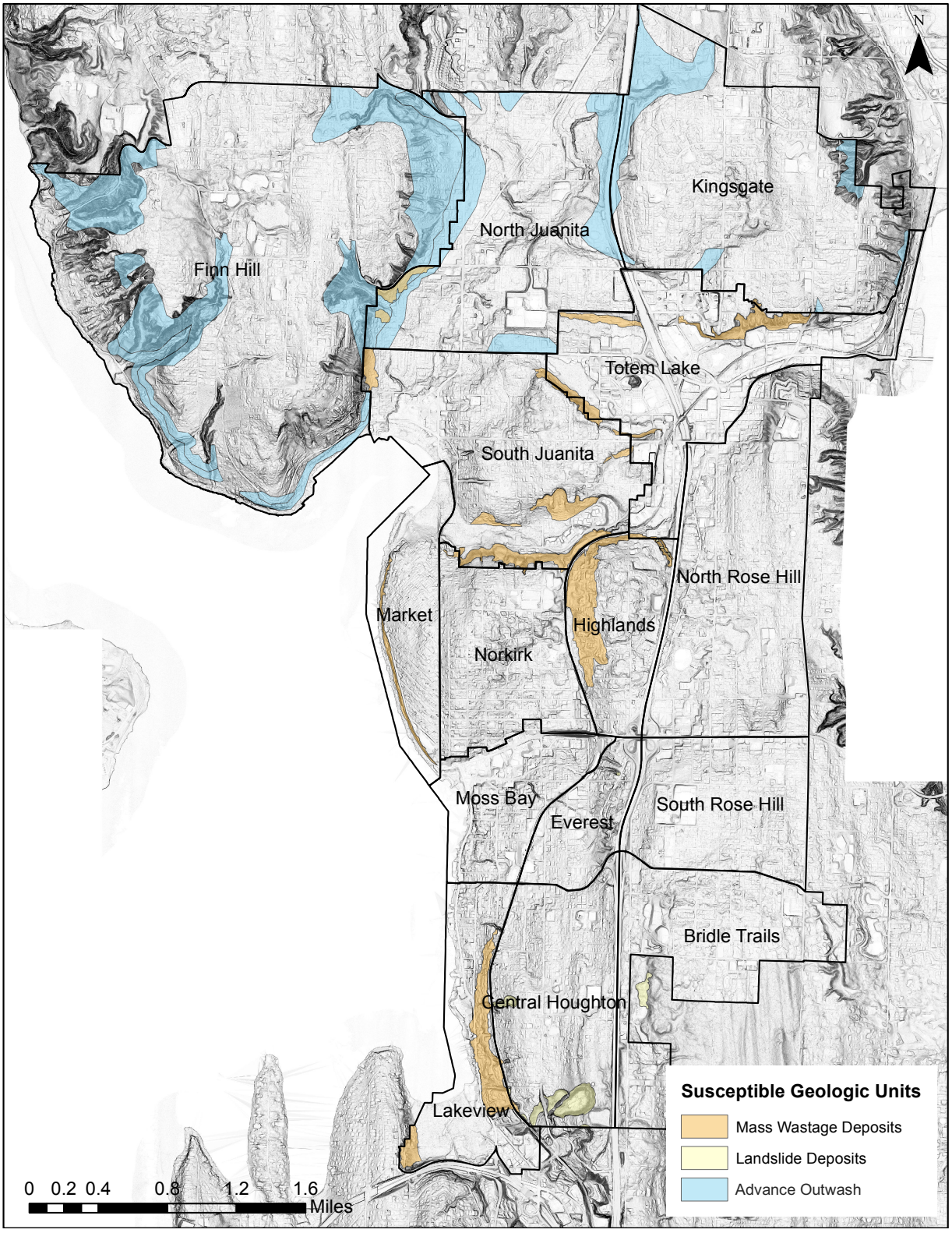

Figure 7. Locations of geologic units particularly susceptible to shallow landslides.

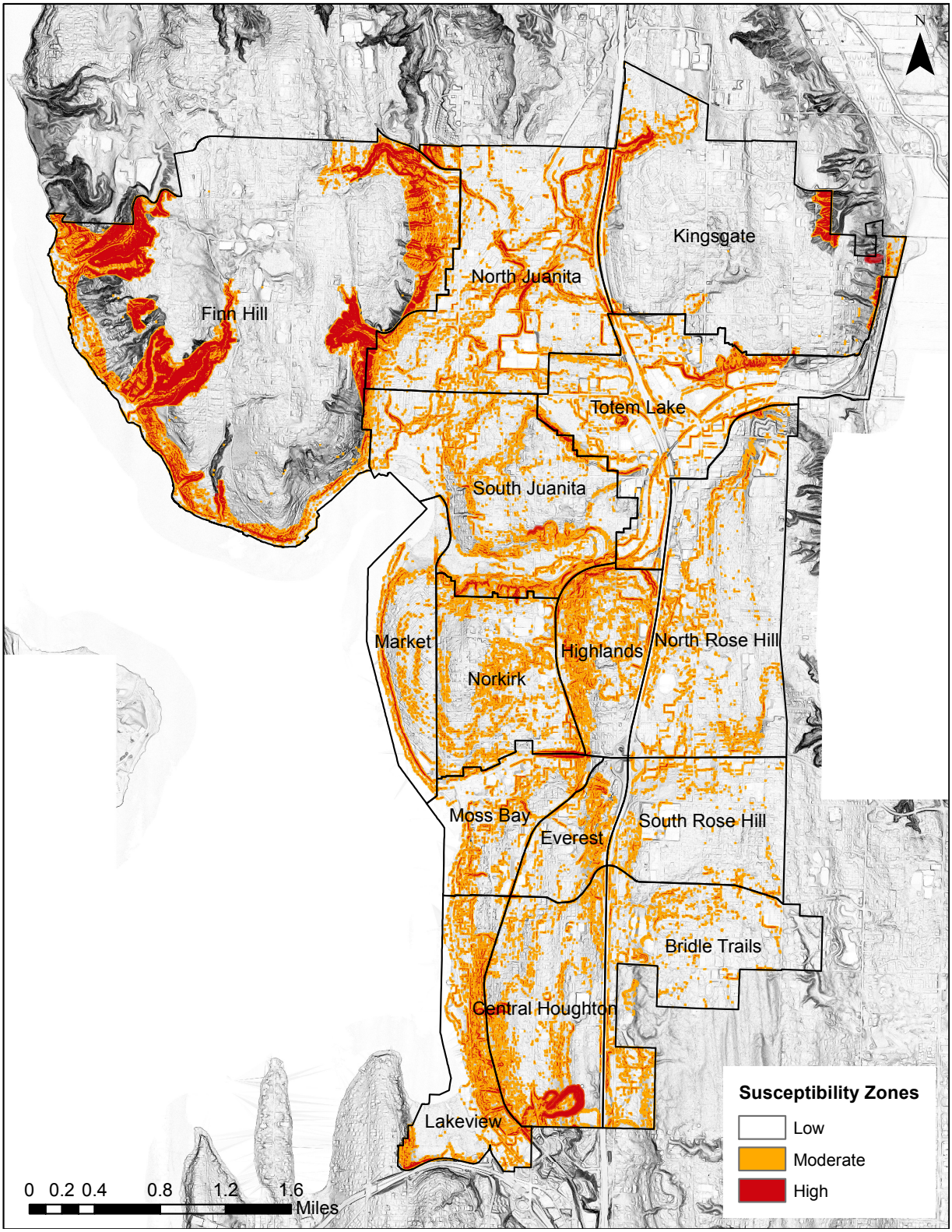

Figure 8. Landslide hazard map of Kirkland, WA. Red areas indicate high hazard for shallow landsliding (FOS<1.25) and orange areas denote moderate hazard (1.25≤FOS≤1.5).

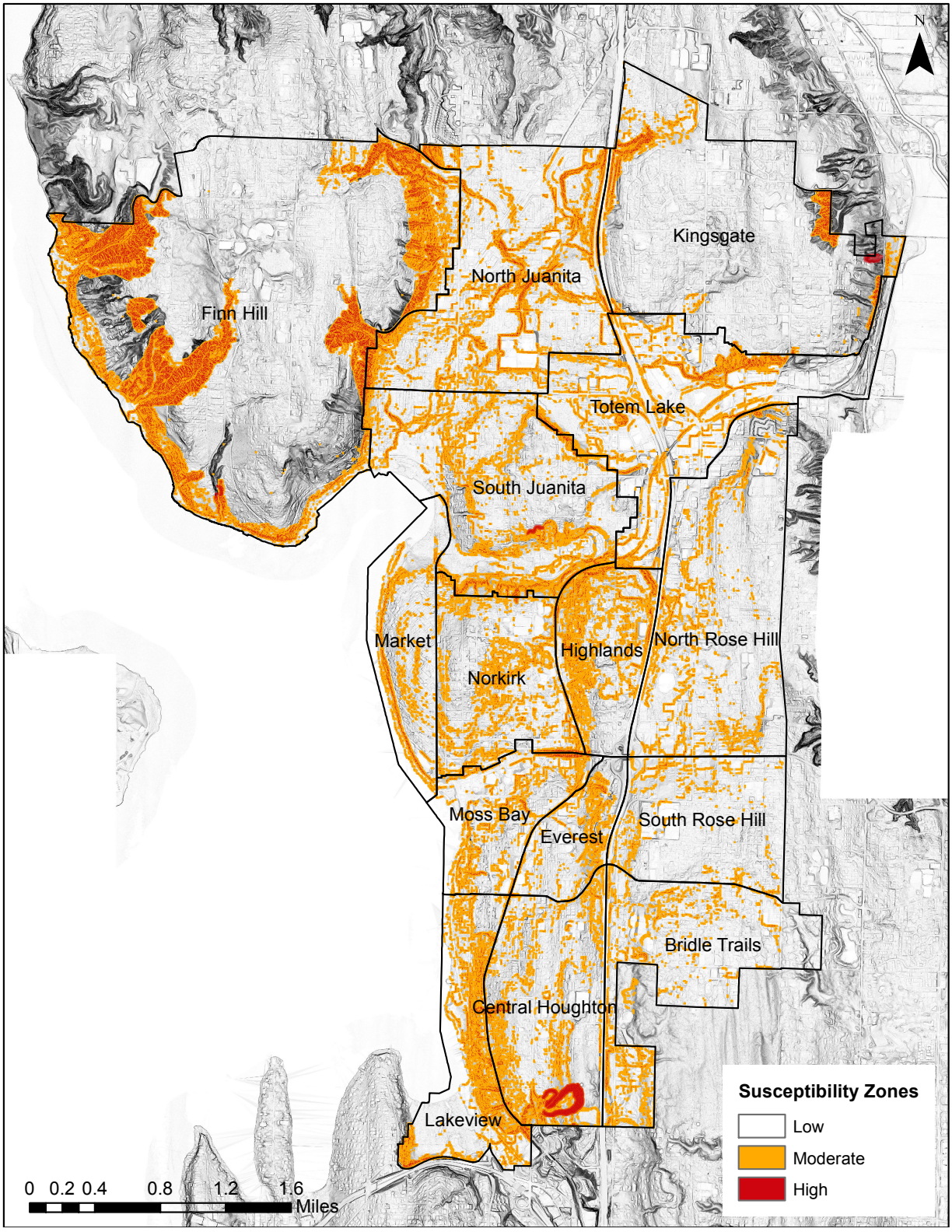

Figure 9. Landslide hazard map of Kirkland, WA with areas of planar or divergent planform curvature removed from the high hazard zones. Red areas are high hazards (FOS<1.25) and orange areas are moderate hazards (1.25≤FOS≤1.5).

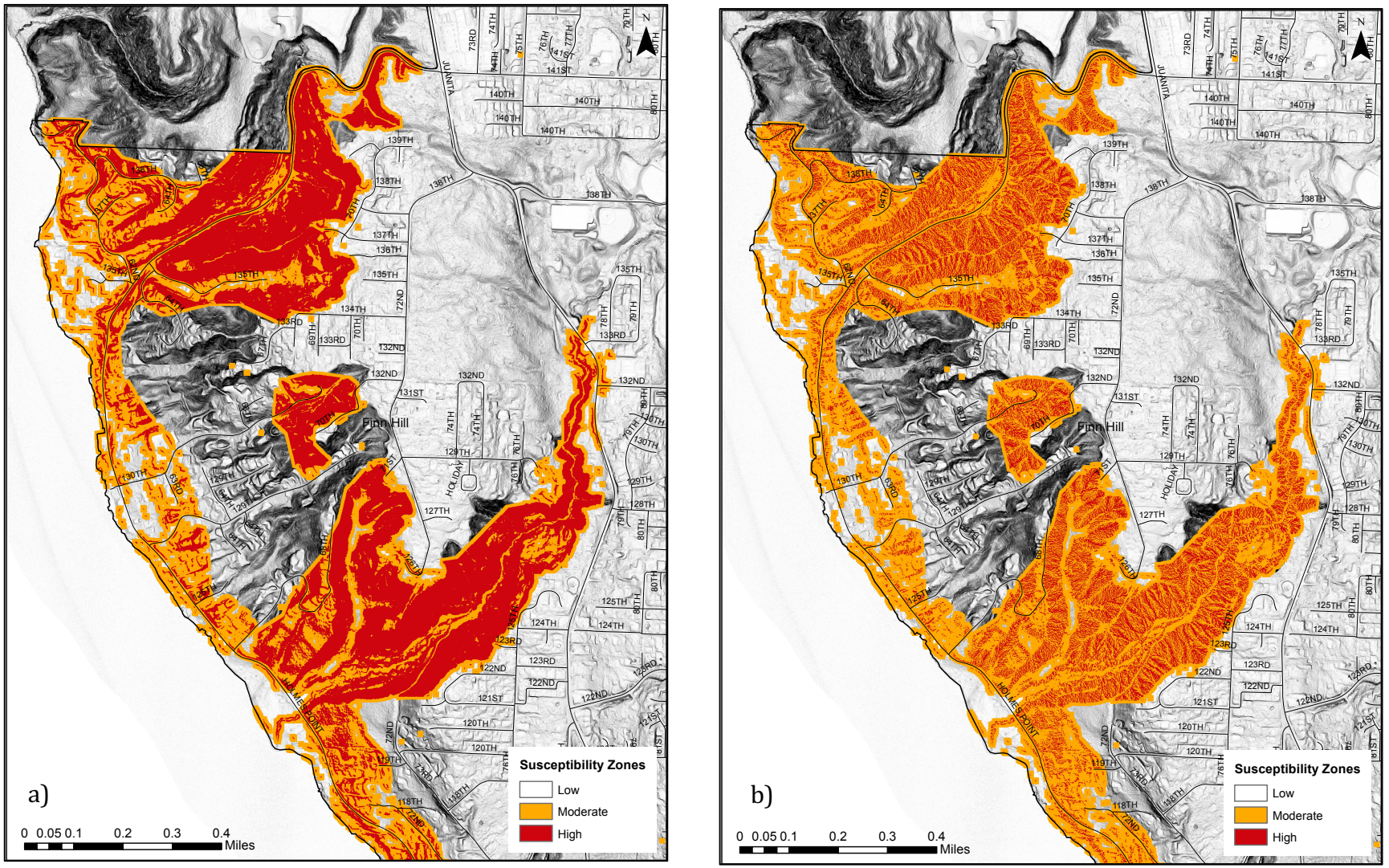

Figure 10. Comparison of hazard areas in gullies on west side of Finn Hill before curvature analysis (a) and after curvature analysis (b).

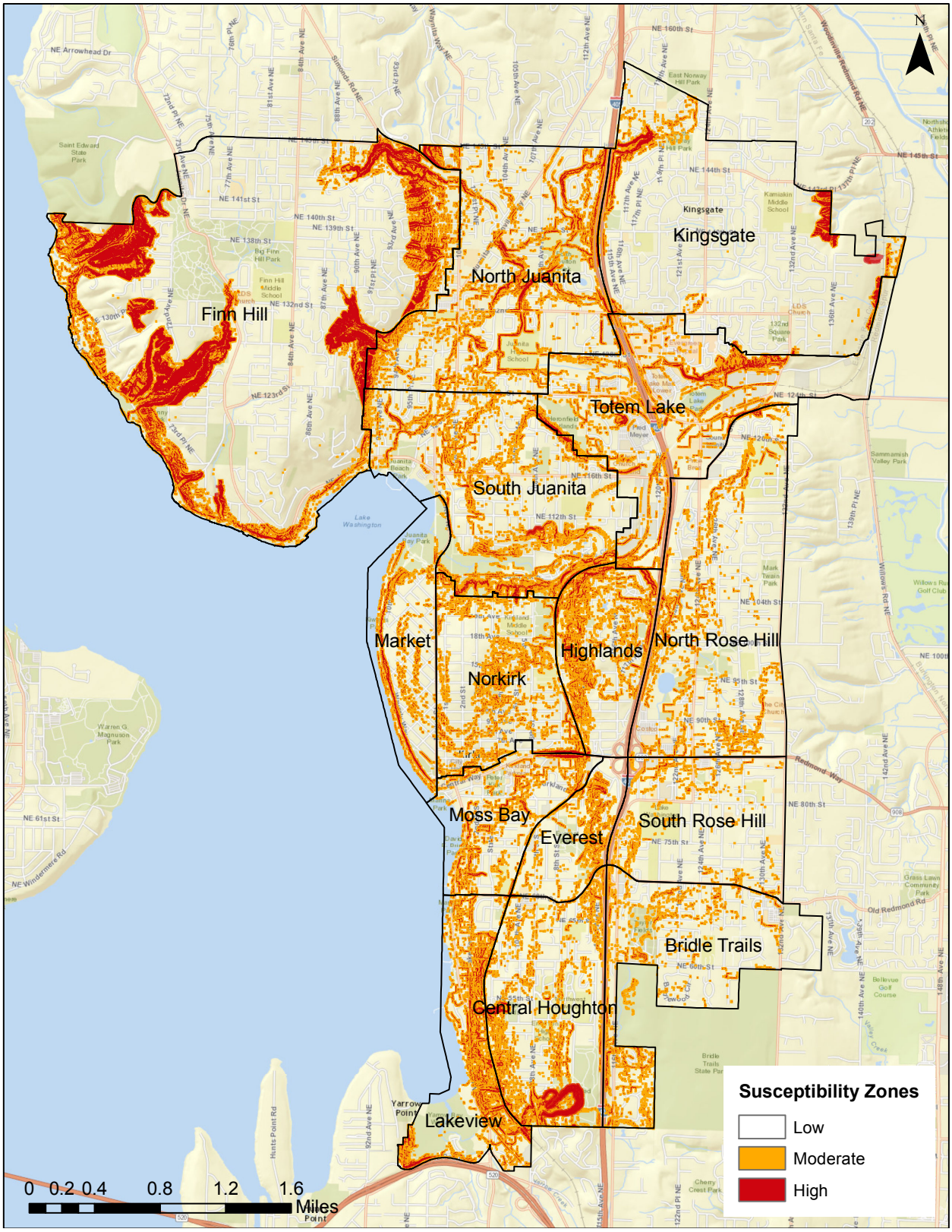

Figure 11. Landslide hazard zones in Kirkland shown in reference to streets and landmarks. Basemap from Esri (2016).

Table 1. Classification of type of material and movement of landslides (Burns and Madin, 2009; Varnes, 1978).

Type of Movement	Type of Material		
	Rock	Debris	Soil
Fall	**RF** rock fall	**DF** debris fall	**EF** earth fall
Topple	**RT** rock topple	**DT** debris topple	**ET** earth topple
Slide-rotational	**RS-R** rock slide-rotational	**DS-R** debris slide-rotational	**ES-R** earth slide-rotational
Slide-translational	**RS-T** rock slide-translational	**DS-T** debris slide-translational	**ES-T** earth slide-translational
Lateral spread	**RSP** rock spread	**DSP** debris spread	**ESP** earth spread
Flow	**RFL** rock flow	**DFL** debris flow	**EFL** earth flow
Complex	**C** complex or combinations of two or more types (for example, ES-R + EFL)		

Table 2. Geotechnical properties of geologic units found in study area (Selby, 1985; Savage, Morrissey, and Baum, 2000; Debray and Savage, 2001; Harp, Michael, and Laprade, 2006).

Legend	
	Selby, 1993
	Savage, Morrissey, and Baum, 2000
	Debray and Savage, 2001
	Harp, Michael, and Laprade, 2006

Geologic Unit	Geologic Unit Label	Raster Value Geologic Code	Angle of Internal Friction (ϕ') (°)	Cohesion (c') (kPa)	Cohesion (lb/ft^2)	Unit Weight (saturated) (KN/m^3)	Unit Weight (saturated) (lb/ft^3)	Slope (°) FOS>1.5	Slope (°) FOS>1.25
NONGLACIAL DEPOSITS (HOLOCENE)									
Alluvium	Qal	8	32	0	0	18.8	119.756	11	13
Fan deposits	Qf	28	30	14.4	301	18.8	119.756	16.5	19.5
Lake deposits	Ql	15	24	19.2	401	18.8	119.756	16.5	19.5
Landslide deposits	Qls	34	32	19.2	401	19	121.03	19.5	23
Mass wastage deposits	Qmw	35	32	19.2	401	19	121.03	19.5	23
Peat and organic-rich deposits	Qp	1	24	24	501	18.8	119.756	18.5	22
Wetland deposits	Qw	32	24	9.6	200	18.8	119.756	12	14.5
Water	water	33	-	-	-	-	-	-	-
OLDER GLACIAL AND NONGLACIAL DEPOSITS (PLEISTOCENE)									
Olympia beds	Qob	16	34	19.2	401	18.8	119.756	20.5	24
Pre-Fraser glaciation age deposits	Qpf	24	34	19.2	401	20	127.4	20.5	24.5
Pre-Fraser fine-grained deposits	Qpff	27	26	28.7	599	20	127.4	21	25.5
Pre-Fraser nonglacial deposits	Qpfn	5	34	19.2	401	20	127.4	20.5	24.5

Geologic Unit	Geologic Unit Label	Raster Value Geologic Code	Angle of Internal Friction (ϕ') (°)	Cohesion (c') (kPa)	Cohesion (lb/ft^2)	Unit Weight (saturated) (KN/m^3)	Unit Weight (saturated) (lb/ft^3)	Slope (°) FOS>1.5	Slope (°) FOS>1.25
Pre-Fraser coarse-grained nonglacial deposits	Qpfnc	18	36	19.2	401	20	127.4	21.5	25.5
Pre-Fraser fine-grained nonglacial deposits	Qpfnf	17	26	28.7	599	20	127.4	21	25.5
Pre-Olympia coarse-grained deposits	Qpoc	20	36	19.2	401	20	127.4	21.5	25.5
Pre-Olympia fine-grained deposits	Qpof	22	26	28.7	599	20	127.4	21	25.5
Pre-Olympia glacial deposits	Qpog	7	33	28.7	599	20	127.4	24	28.5
Pre-Olympia coarse-grained glacial deposits	Qpogc	29	38	19.2	401	20	127.4	22.5	26.5
Pre-Olympia gine-grained glacial deposits	Qpogf	30	26	28.7	599	20	127.4	21	25.5
Pre-Olympia glacial till	Qpogt	6	33	95.8	2000	20	127.4	55	69
Pre-Olympia nonglacial deposits	Qpon	19	34	19.2	401	20	127.4	20.5	24.5
Pre-Olympia coarse-grained nonglcial deposits	Qponc	21	36	19.2	401	20	127.4	21.5	25.5
Continental glacial drift, pre-Fraser, and nonglacial deposits	Qgpc	43	34	19.2	401	18.8	119.756	20.5	24
Continental sedimentary deposits or rocks, conglomerate	Qcg	42	25	1000	20880	18.8	119.756	-	-
YOUNGER GLACIAL DEPOSITS (FRASER GLACIATION, PLEISTOCENE)									
Vashon advance outwash deposits	Qva	13	38	19.2	401	19.2	122.304	22	26.5
Vashon ice-contact deposits	Qvi	11	30	28.7	599	18.8	119.756	23	27.5

Geologic Unit	Geologic Unit Label	Raster Value Geologic Code	Angle of Internal Friction (ϕ') (°)	Cohesion (c') (kPa)	Cohesion (lb/ft^2)	Unit Weight (saturated) (KN/m^3)	Unit Weight (saturated) (lb/ft^3)	Slope (°) FOS>1.5	Slope (°) FOS>1.25
Lawton Clay member of the Vashon Drift	Qvlc	12	26	28.7	599	20	127.4	21	25.5
Vashon recessional outwash deposits	Qvr	3	34	14.4	301	18.8	119.756	18	21.5
Vashon recessional lacustrine deposits	Qvrl	14	24	19.2	401	18.8	119.756	16.5	19.5
Vashon recessional Lake Bretz deposits	Qvrlb	4	24	19.2	401	18.8	119.756	16.5	19.5
Vashon recessional Lake Bridal Trails deposits	Qvrlbt	31	24	19.2	401	18.8	119.756	16.5	19.5
Vashon recessional Lake Forbes deposits	Qvrlf	10	24	19.2	401	18.8	119.756	16.5	19.5
Vashon recessional Lake Juanita deposits	Qvrlj	26	24	19.2	401	18.8	119.756	16.5	19.5
Vashon recessional lacustrine deposits (organic)	Qvrlo	2	24	21.5	449	18.8	119.756	16.5	19.5
Vashon recessional Lake Russell deposits	Qvrlr	25	24	19.2	401	18.8	119.756	16.5	19.5
Vashon recessional Lake Totem deposits	Qvrlt	23	24	19.2	401	18.8	119.756	16.5	19.5
Vashon subglacial till	Qvt	9	33	95.8	2000	18.8	119.756	58	73.5
Advance continental glacial outwash, Fraser-age	Qga	37	32	0	0	19.2	122.304	11	13.5
Advance continental glacial outwash, Fraser-age, transitional beds of Menard (1985)	Qga(t)	38	32	0	0	19.2	122.304	11	13.5

Geologic Unit	Geologic Unit Label	Raster Value Geologic Code	Angle of Internal Friction (ϕ') (°)	Cohesion (c') (kPa)	Cohesion (lb/ft^2)	Unit Weight (saturated) (KN/m^3)	Unit Weight (saturated) (lb/ft^3)	Slope (°) FOS>1.5	Slope (°) FOS>1.25
Continental glacial till, Fraser-age, mostly Vashon Stade	Qgt	39	33	95.8	2000	18.8	119.756	58	73.5
Continental glacial outwash, Fraser-age, mostly Vashon stade	Qgo	40	30	0	0	18.8	119.756	10	12
Glacial drift, undivided	Qgu	41	24	19.2	401	18.8	119.756	16.5	19.5

Table 3. Counts of high and moderate hazard areas in the landslide hazard map without curvature clipping.

Landslide Hazard Map

Layer	High Hazard (Number of Cells)	High Hazard (Total Area, ft^2)	Mod. Hazard (Number of Cells)	Mod. Hazard (Total Area, ft^2)
Deposits	8,642	77,778	-	-
Scarps	75,480	679,320	-	-
Relief-Clipped FOS Map	31,811	286,299	52,200	469,800
FOS Buffer Map	-	-	156,985	1,412,865
Total	115,933	1,043,397	209,185	1,882,665

Table 4. Counts of high and moderate hazard areas in the landslide hazard map with curvature clipping.

Landslide Hazard Map with Curvature

Layer	High Hazard (Number of Cells)	High Hazard (Total Area, ft^2)	Mod. Hazard (Number of Cells)	Mod. Hazard (Total Area, ft^2)
Deposits	8,642	77,778	-	-
Scarps	75,480	679,320	-	-
Relief- and Curvature-Clipped FOS Map	15,616	140,544	25,669	231,021
FOS Buffer Map	-	-	150,038	1,350,342
Total	99,738	897,642	175,707	1,581,363

Appendix A

Landslide inventory, divided into three tiles (NW, NE, S).

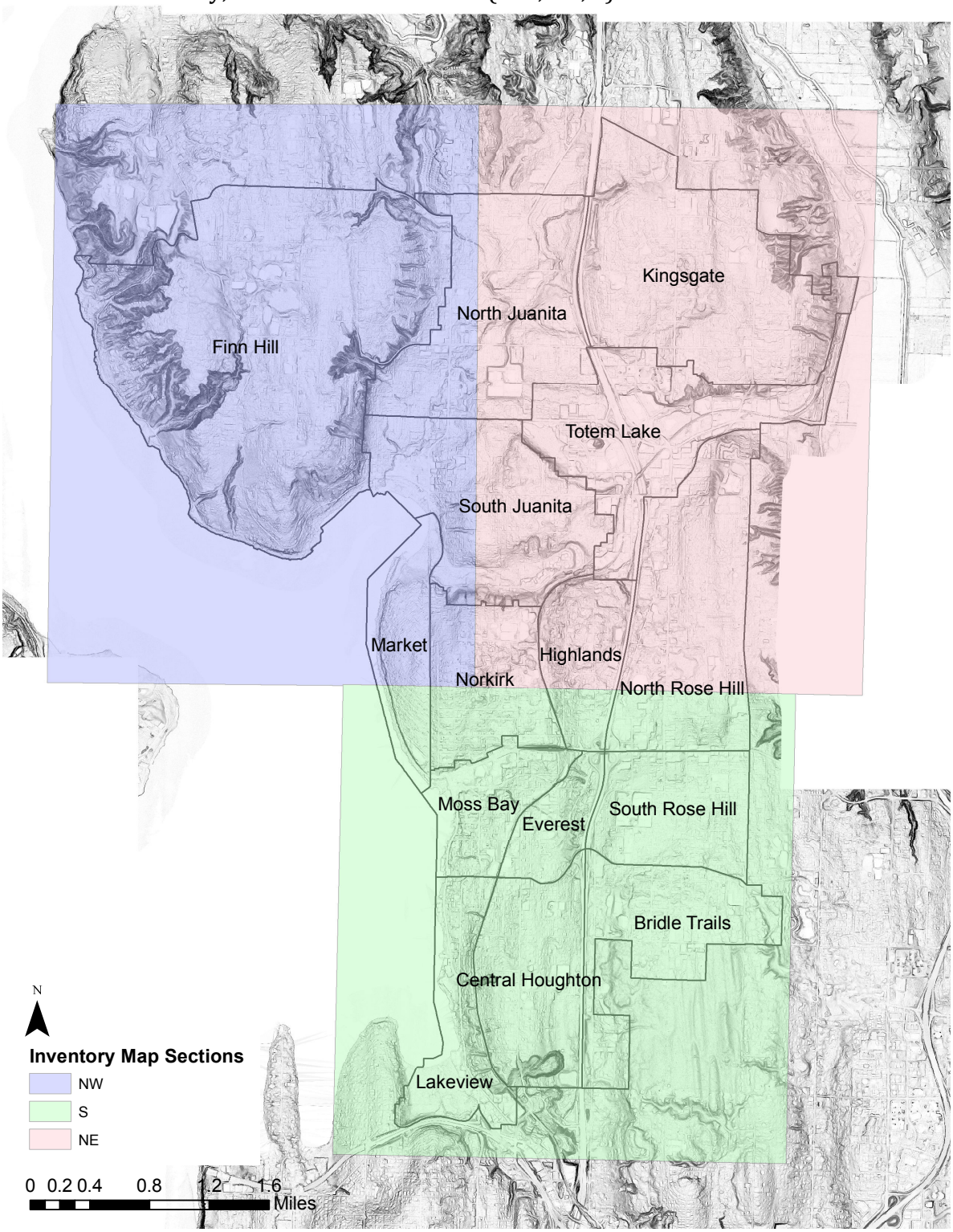

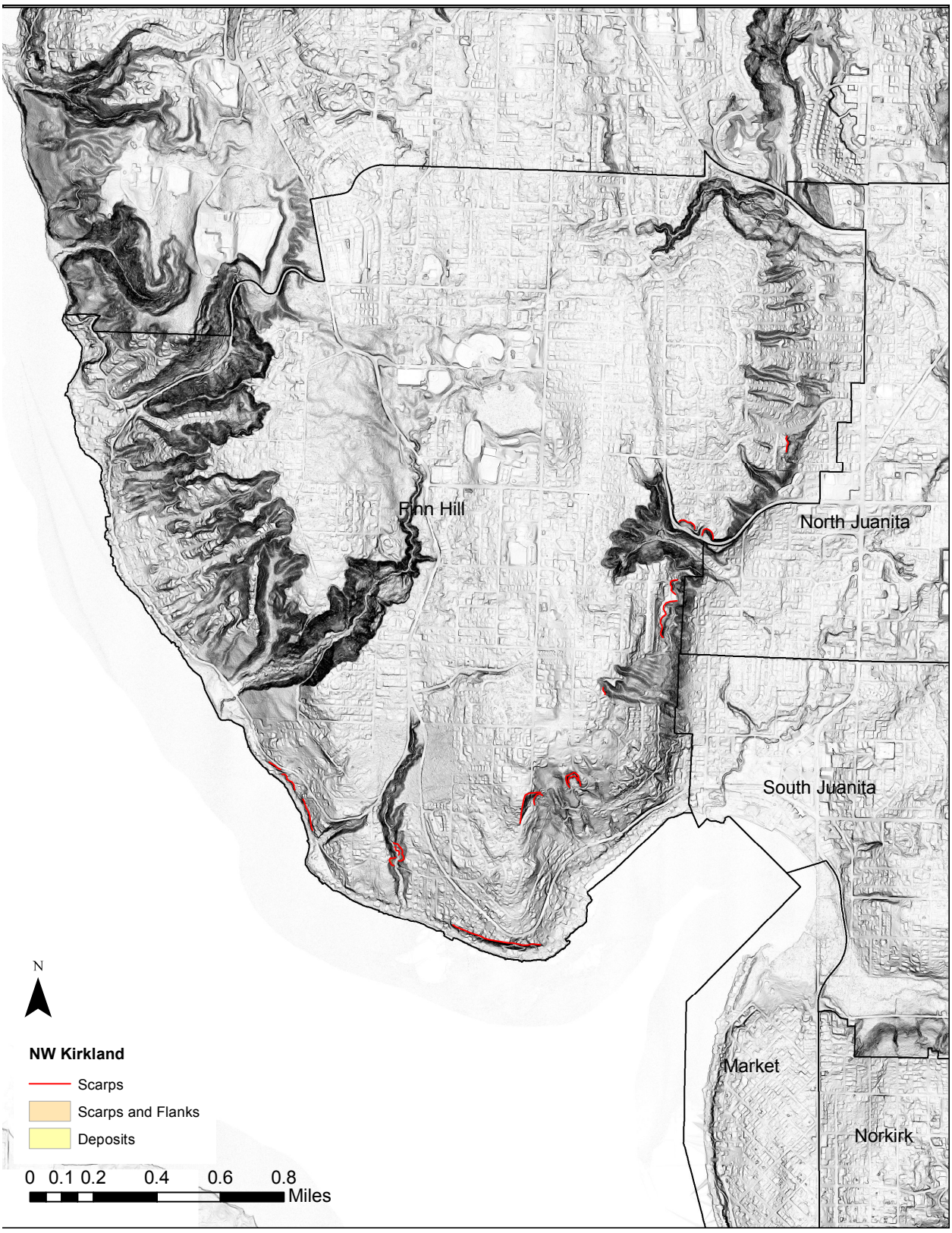
Finn Hill
North Juanita
South Juanita
Market
Norkirk
N
NW Kirkland
Scarps
Scarps and Flanks
Deposits
0 0.1 0.2 0.4 0.6 0.8
Miles

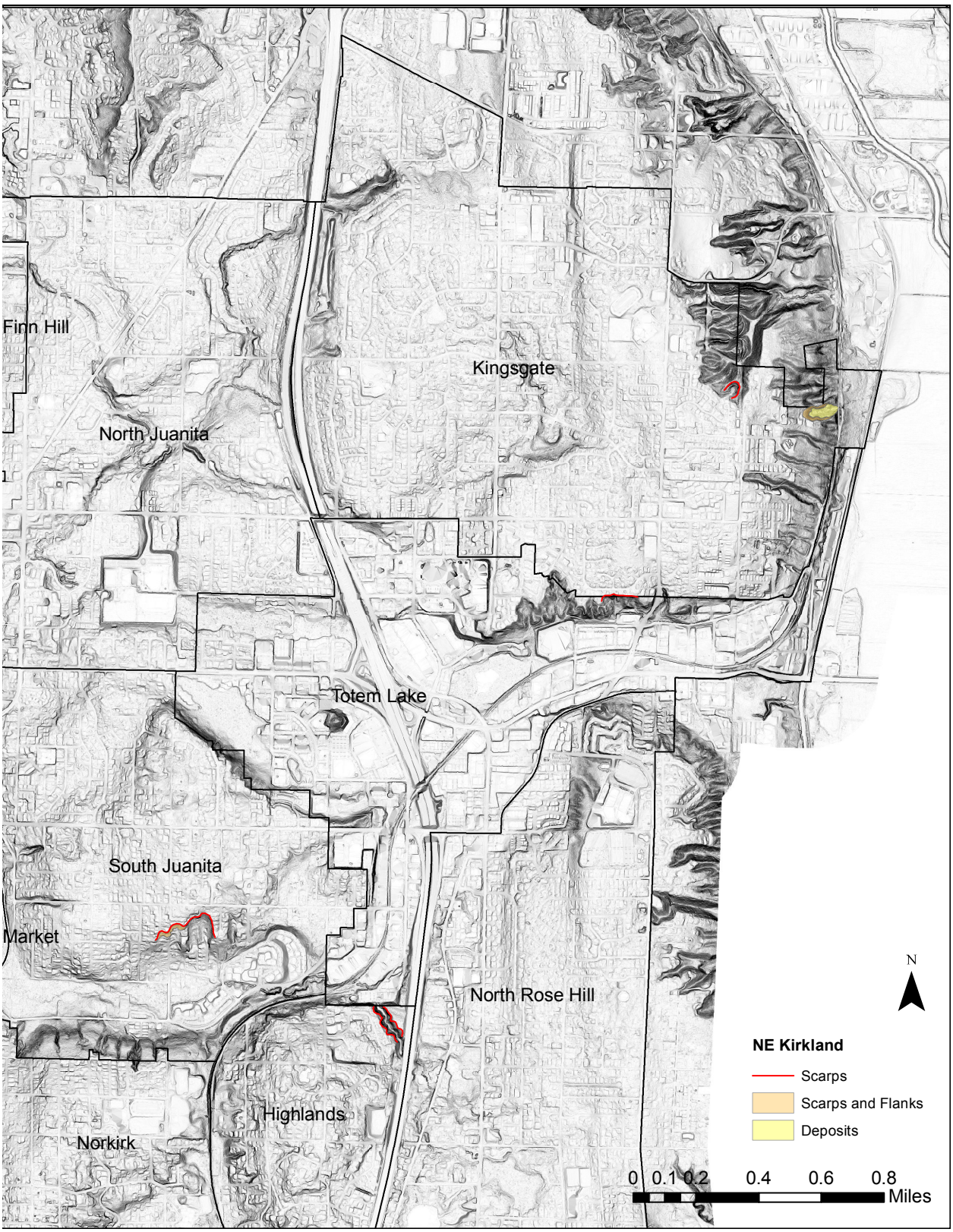
Finn Hill
Kingsgate
North Juanita
Totem Lake
South Juanita
Market
North Rose Hill
Highlands
Norkirk
N
NE Kirkland
Scarps
Scarps and Flanks
Deposits
0 0.1 0.2 0.4 0.6 0.8
Miles

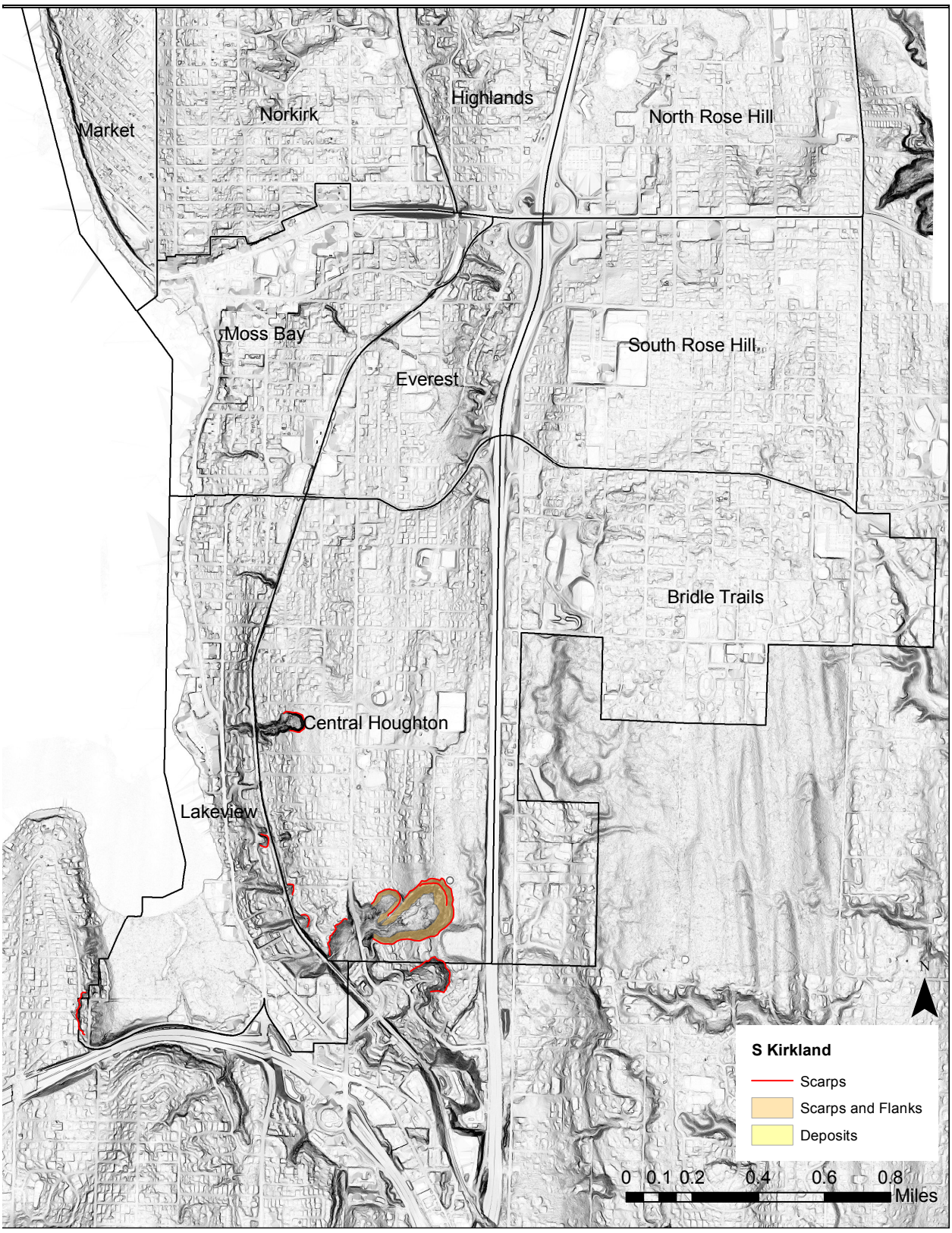
Market
Norkirk
Highlands
North Rose Hill
Moss Bay
Everest
South Rose Hill
Bridle Trails
Central Houghton
Lakeview
N
S Kirkland
Scarps
Scarps and Flanks
Deposits
0 0.1 0.2 0.4 0.6 0.8
Miles

Appendix B

Example of FOS calculation spreadsheet for geologic unit Qal (a similar spreadsheet was created for each unit). Inputs to FOS equation are listed in the upper left table. FOS is split into three portions (Eqn. 3, Eqn. 4, and Eqn. 5), and these three calculations are combined to find the final FOS value for every slope. Slopes that produce a FOS of 1.25 and 1.5 are highlighted in yellow.

Qal

Effective cohesion	**c'**	0	lb/ft2
Effective internal friction	**Φ'**	32	
Unit weight (soil)	**γ(b)**	119.756	lb/ft3
Unit weight (water)	**γ(w)**	64	lb/ft3
Depth to failure surface	**t**	15.0	ft
Proportion of slope thckness saturated	**m**	1.0	
Slope	**θ**	see table below	deg.

FOS Calculation	
Eqn. 3	$\frac{c'}{\gamma h sin\theta}$
Eqn. 4	$\frac{tan\phi'}{tan\theta}$
Eqn. 5	$\frac{m\gamma_w tan\phi'}{\gamma tan\theta}$
FOS	$FOS = (\text{Eqn. 3}) + (\text{Eqn. 4}) - (\text{Eqn. 5})$

Slope (θ)	Eqn. 3	Eqn. 4	Eqn. 5	FOS
1.0	0.00	35.8	19.1	16.67
1.5	0.00	23.9	12.8	11.11
2.0	0.00	17.9	9.6	8.33
2.5	0.00	14.3	7.6	6.66
3.0	0.00	11.9	6.4	5.55
3.5	0.00	10.2	5.5	4.76
4.0	0.00	8.9	4.8	4.16
4.5	0.00	7.9	4.2	3.70
5.0	0.00	7.1	3.8	3.33
5.5	0.00	6.5	3.5	3.02
6.0	0.00	5.9	3.2	2.77
6.5	0.00	5.5	2.9	2.55
7.0	0.00	5.1	2.7	2.37
7.5	0.00	4.7	2.5	2.21
8.0	0.00	4.4	2.4	2.07
8.5	0.00	4.2	2.2	1.95
9.0	0.00	3.9	2.1	1.84
9.5	0.00	3.7	2.0	1.74
10.0	0.00	3.5	1.9	1.65
10.5	0.00	3.4	1.8	1.57
11.0	0.00	3.2	1.7	1.50
11.5	0.00	3.1	1.6	1.43
12.0	0.00	2.9	1.6	1.37
12.5	0.00	2.8	1.5	1.31
13.0	0.00	2.7	1.4	1.26
13.5	0.00	2.6	1.4	1.21
14.0	0.00	2.5	1.3	1.17
14.5	0.00	2.4	1.3	1.12
15.0	0.00	2.3	1.2	1.09
15.5	0.00	2.3	1.2	1.05
16.0	0.00	2.2	1.2	1.01
16.5	0.00	2.1	1.1	0.98
17.0	0.00	2.0	1.1	0.95
17.5	0.00	2.0	1.1	0.92
18.0	0.00	1.9	1.0	0.90
18.5	0.00	1.9	1.0	0.87
19.0	0.00	1.8	1.0	0.84
19.5	0.00	1.8	0.9	0.82
20.0	0.00	1.7	0.9	0.80

Slope (θ)	Eqn. 3	Eqn. 4	Eqn. 5	FOS
20.5	0.00	1.7	0.9	0.78
21.0	0.00	1.6	0.9	0.76
21.5	0.00	1.6	0.8	0.74
22.0	0.00	1.5	0.8	0.72
22.5	0.00	1.5	0.8	0.70
23.0	0.00	1.5	0.8	0.69
23.5	0.00	1.4	0.8	0.67
24.0	0.00	1.4	0.8	0.65
24.5	0.00	1.4	0.7	0.64
25.0	0.00	1.3	0.7	0.62
25.5	0.00	1.3	0.7	0.61
26.0	0.00	1.3	0.7	0.60
26.5	0.00	1.3	0.7	0.58
27.0	0.00	1.2	0.7	0.57
27.5	0.00	1.2	0.6	0.56
28.0	0.00	1.2	0.6	0.55
28.5	0.00	1.2	0.6	0.54
29.0	0.00	1.1	0.6	0.52
29.5	0.00	1.1	0.6	0.51
30.0	0.00	1.1	0.6	0.50
30.5	0.00	1.1	0.6	0.49
31.0	0.00	1.0	0.6	0.48
31.5	0.00	1.0	0.5	0.47
32.0	0.00	1.0	0.5	0.47
32.5	0.00	1.0	0.5	0.46
33.0	0.00	1.0	0.5	0.45
33.5	0.00	0.9	0.5	0.44
34.0	0.00	0.9	0.5	0.43
34.5	0.00	0.9	0.5	0.42
35.0	0.00	0.9	0.5	0.42
35.5	0.00	0.9	0.5	0.41
36.0	0.00	0.9	0.5	0.40
36.5	0.00	0.8	0.5	0.39
37.0	0.00	0.8	0.4	0.39
37.5	0.00	0.8	0.4	0.38
38.0	0.00	0.8	0.4	0.37
38.5	0.00	0.8	0.4	0.37
39.0	0.00	0.8	0.4	0.36
39.5	0.00	0.8	0.4	0.35

Slope (θ)	Eqn. 3	Eqn. 4	Eqn. 5	FOS
40.0	0.00	0.7	0.4	0.35
40.5	0.00	0.7	0.4	0.34
41.0	0.00	0.7	0.4	0.33
41.5	0.00	0.7	0.4	0.33
42.0	0.00	0.7	0.4	0.32
42.5	0.00	0.7	0.4	0.32
43.0	0.00	0.7	0.4	0.31
43.5	0.00	0.7	0.4	0.31
44.0	0.00	0.6	0.3	0.30
44.5	0.00	0.6	0.3	0.30
45.0	0.00	0.6	0.3	0.29
45.5	0.00	0.6	0.3	0.29
46.0	0.00	0.6	0.3	0.28
46.5	0.00	0.6	0.3	0.28
47.0	0.00	0.6	0.3	0.27
47.5	0.00	0.6	0.3	0.27
48.0	0.00	0.6	0.3	0.26
48.5	0.00	0.6	0.3	0.26
49.0	0.00	0.5	0.3	0.25
49.5	0.00	0.5	0.3	0.25
50.0	0.00	0.5	0.3	0.24
50.5	0.00	0.5	0.3	0.24
51.0	0.00	0.5	0.3	0.24
51.5	0.00	0.5	0.3	0.23
52.0	0.00	0.5	0.3	0.23
52.5	0.00	0.5	0.3	0.22
53.0	0.00	0.5	0.3	0.22
53.5	0.00	0.5	0.2	0.22
54.0	0.00	0.5	0.2	0.21
54.5	0.00	0.4	0.2	0.21
55.0	0.00	0.4	0.2	0.20
55.5	0.00	0.4	0.2	0.20
56.0	0.00	0.4	0.2	0.20
56.5	0.00	0.4	0.2	0.19
57.0	0.00	0.4	0.2	0.19
57.5	0.00	0.4	0.2	0.19
58.0	0.00	0.4	0.2	0.18
58.5	0.00	0.4	0.2	0.18
59.0	0.00	0.4	0.2	0.17
59.5	0.00	0.4	0.2	0.17
60.0	0.00	0.4	0.2	0.17
60.5	0.00	0.4	0.2	0.16
61.0	0.00	0.3	0.2	0.16
61.5	0.00	0.3	0.2	0.16
62.0	0.00	0.3	0.2	0.15
62.5	0.00	0.3	0.2	0.15
63.0	0.00	0.3	0.2	0.15
63.5	0.00	0.3	0.2	0.15
64.0	0.00	0.3	0.2	0.14
64.5	0.00	0.3	0.2	0.14
65.0	0.00	0.3	0.2	0.14

Slope (θ)	Eqn. 3	Eqn. 4	Eqn. 5	FOS
65.5	0.00	0.3	0.2	0.13
66.0	0.00	0.3	0.1	0.13
66.5	0.00	0.3	0.1	0.13
67.0	0.00	0.3	0.1	0.12
67.5	0.00	0.3	0.1	0.12
68.0	0.00	0.3	0.1	0.12
68.5	0.00	0.2	0.1	0.11
69.0	0.00	0.2	0.1	0.11
69.5	0.00	0.2	0.1	0.11
70.0	0.00	0.2	0.1	0.11
70.5	0.00	0.2	0.1	0.10
71.0	0.00	0.2	0.1	0.10
71.5	0.00	0.2	0.1	0.10
72.0	0.00	0.2	0.1	0.09
72.5	0.00	0.2	0.1	0.09
73.0	0.00	0.2	0.1	0.09
73.5	0.00	0.2	0.1	0.09
74.0	0.00	0.2	0.1	0.08
74.5	0.00	0.2	0.1	0.08
75.0	0.00	0.2	0.1	0.08
75.5	0.00	0.2	0.1	0.08
76.0	0.00	0.2	0.1	0.07
76.5	0.00	0.2	0.1	0.07
77.0	0.00	0.1	0.1	0.07
77.5	0.00	0.1	0.1	0.06
78.0	0.00	0.1	0.1	0.06
78.5	0.00	0.1	0.1	0.06
79.0	0.00	0.1	0.1	0.06
79.5	0.00	0.1	0.1	0.05
80.0	0.00	0.1	0.1	0.05
80.5	0.00	0.1	0.1	0.05
81.0	0.00	0.1	0.1	0.05
81.5	0.00	0.1	0.0	0.04
82.0	0.00	0.1	0.0	0.04
82.5	0.00	0.1	0.0	0.04
83.0	0.00	0.1	0.0	0.04
83.5	0.00	0.1	0.0	0.03
84.0	0.00	0.1	0.0	0.03
84.5	0.00	0.1	0.0	0.03
85.0	0.00	0.1	0.0	0.03
85.5	0.00	0.0	0.0	0.02
86.0	0.00	0.0	0.0	0.02
86.5	0.00	0.0	0.0	0.02
87.0	0.00	0.0	0.0	0.02
87.5	0.00	0.0	0.0	0.01
88.0	0.00	0.0	0.0	0.01
88.5	0.00	0.0	0.0	0.01
89.0	0.00	0.0	0.0	0.01
89.5	0.00	0.0	0.0	0.00
90.0	0.00	0.0	0.0	0.00